This is a previous version of the article published in Chemical Engineering Science. 2016, 155: 482-503. doi:10.1016/j.ces.2016.09.005

Analysis of the state equations of a real gas at high pressures with the virial coefficients obtained from controlled chaotic oscillations

Manuel F. Pérez-Polo[a*], Manuel Pérez-Molina[a], Elena Fernández Varó[b], Javier Gil Chica[a]

[a] Departamento de Física, Ingeniería de Sistemas y Teoría de la Señal, Escuela Politécnica Superior, Universidad de Alicante. [b] Departamento de Óptica, Campus de San Vicente, Alicante, Spain. Fax 965903682. [a*]E-mail: manolo@dfists.ua.es. [b]E-mail: ma_perez_m@hotmail.com. [c]E-mail: elena.fernandez@ua.es. [d]E-mail: gil@dfists.ua.es. Phone: +34 965909673

Abstract

This paper investigates several cubic and non-cubic state equations of real gases at high pressures by using the virial coefficients estimated from chaotic oscillations with a mechanical-thermal device. The mechanical part is formed by a cylinder with a piston whose motion is limited by means of a nonlinear spring, a damper and a nonlinear control force to decouple the mechanical and thermal subsystems. To maintain the gas temperature approximately constant, a linear PI controller and a nonlinear control law which manipulates the flow rate of two heating coils inside the cylinder are added. The stability of the mechanical subsystem is analyzed through the first Lyapunov value, whose harmonic variation leads to chaotic behavior with great pressures and an almost constant temperature. The chaotic simulations for nonpolar gases are treated like experimental data to obtain an arbitrary number of virial coefficients which reproduce the state equation in a prescribed pressure range. The validity of the proposed device has been corroborated by using another alternative route to chaos and calculating the fugacity coefficient. The analytical calculations are in good agreement with the numerical simulations.

Keywords: State equations, first Lyapunov value, chaotic oscillations, virial coefficients, linear and nonlinear control.

a* Author whose correspondence should be addressed

1 Introduction

In the analysis and design of chemical processes, the pressure of a real gas can be described as the sum of the pressure of an ideal one plus a series expansion in terms of densities or specific volumes. The coefficients of such expansion are known as virial coefficients, which only depend on the gas temperature and the potential interaction energy between the molecules (Prausnitz, et al.,2000; Goodwin et al., 2010). For most fluids, only the first and second virial coefficients are experimentally known (Dymond et al., 1980; Dymond et al., 2002).

A state equation based on the virial expansion has been applied at relatively low pressures (Mason et al., 1968; Annamalai et al., 2002), for which the two first coefficients provide the required precision for the applications. On the other hand, one of the advantages of the virial expansion is that it can be easily obtained for a gaseous mixture through simple combining rules from the virial coefficients of each of the gases present in the mixture (Prausnitz, et al., 2000; Poling et al. 2001).

In this work we analyze the behavior and the precision of several cubic and non-cubic state equations when these equations are expanded in terms of virial coefficients. Reviews of such equations with and without translate volume can be found in Refs (Poling et al. 2001; Abbot, 1979; Tsonopoulos et al., 1985; Wei et al., 2000; Valderrama, 2003) showing their advantages and disadvantages. The considered cubic equations in this paper are: i) Redlich-Wong (RK) (Redlich et al., 1948), ii) Soave_Redlich-Kwong (SRK) (Soave, 1972), iii) Peng-Robinson (PR) (Peng et al., 1976), iv) Peng-Robinson with translate volume (Tassios, 1993) and v) Van der Waals with translate volume (VDWt) (Tassios, 1993; Soave, 1984). The considered non-cubic equations are: vi) Beattie-Bridgeman (BB) state equation (Beattie et al., 1927; Su et al., 1946; Hougen et al. 1954) and vii) Empirical state equation of high precision (HP) (Goodwin et al., 2010; Span, 2000; Gmehling et al., 2012). All the previous state equations are analyzed by using methane, nitrogen, oxygen and argon.

On the other hand, the device considered in this paper is a mechanical-thermal system formed by an adiabatic cylinder enclosing a real gas and a mobile piston moving along the cylinder axis. The piston is anchored to the cylinder through a nonlinear

spring and a viscous damper. The thermal subsystem is formed by two heating coils inside the cylinder with the purpose of transferring heat to the gas. An external control force acts on the piston, thus balancing all the forces to maintain the piston motion within the cylinder limits as well for decoupling the mechanical and thermal subsystems. Two additional control devices are applied to the thermal subsystem: one is a linear PI controller and the other is a nonlinear control law for the heat supply by the helical coils by manipulating their flow rate. The purpose of these control devices is to maintain the gas temperature approximately constant (Albertos et al., 2004; Pérez-Molina et al., 2016).

The parameter values and the control laws have been chosen to obtain three equilibrium points. One of them is always a saddle and the other two are weak focuses, whose stability is analyzed by calculating the sign of the first Lyapunov value (Guckenheimer et al., 1983; Wiggins, 2000; Pérez-Polo et al., 2014). With the harmonic variation of the first Lyapunov value between negative values (stable weak focus) and positive values (unstable weak focus) the piston position jumps from one weak focus to the other one, thus providing a route to chaotic oscillations. Furthermore, the chaotic behavior is characterized by a great excursion in the pressure values, whereas the gas temperature remains approximately constant because of the control system.

The chaotic behavior is exploited to obtain a dense set of simulation data which allow estimating the virial coefficients. In order to assure the presence of chaos, the sensitive dependence, all the Lyapunov exponents and the spectral power density have been calculated, thus corroborating also the accuracy of the simulation results (Guckenheimer et al., 1983; Wiggins, 2000; Lichtenberg et al., 1992). By using polynomial least square adjustment, the pressures, temperatures and specific volumes of the gas, a desired number of virial coefficients are obtained for each state equation.

The pressure errors between the virial approximation and the exact equation have been compared, which has allowed estimating an admissible range of pressures for each state equation taking the one of high precision (HP) as a reference. It should be emphasized that the methodology presented in this work admits the use of other state equations, such as the one of reference (Valderrama, 1990). Finally, a discussion

regarding the applicability of the proposed model is presented taking into account another route to chaos and the fugacity coefficient of the methane.

2. Description of the system and mathematical model

The system is formed by a closed cylinder enclosing a non polar real gas (e.g. nitrogen, argon, methane etc.) to which a mobile piston of mass *m* is anchored by means of a nonlinear spring and a damper. The scheme of the device including the control loops is shown in Fig 1. In the control loop 1, the gas temperature *T(t)* is measured, it is transmitted by the TT1 device and compared with the desired gas temperature T_s to generate the error signal $e(t) = T_s - T(t)$. Such error signal actuates on a TIC temperature controller to generate a proportional plus integral (PI) control signal on the CV_1 control valve. The purpose of this control loop 1 is to maintain the gas temperature as constant as possible with only small oscillations around the temperature set point T_s. The control loop 2 is nonlinear and has two input signals which are proportional to *e(t)* and the flow rate $F_v(t)$, which is measured and transmitted by a FT device. The sum of these signals are transmitted to the control valve CV_2 through a nonlinear device defined by the function *f(t)*. On the other hand, the aim of the control loop 2 is to stabilize the thermal subsystem.

The bumpers *B* provide a non-accessible volume for the piston where there are two helical coils *C* and C_1 with the goal of heating the gas. It is assumed that the net force of the spring for the distance d_1 is zero. In addition, such spring is considered to be nonlinear with coefficients K_1 and K_2, whereas the damper is assumed to be linear with damping coefficient *b*. The external control force $F'(t) + F_s$ is applied to ensure a piston motion within the cylinder limits and to obtain a desired gas behavior. The parameter values are indicated in the legend of Fig 1, and their physical meaning is discussed in Ref (Pérez-Molina et al., 2016). Since the device is formed by a coupled mechanical-thermal subsystem, the model equations and the equilibrium points are discussed separately for each subsystem as follows.

Figure 1

2.1 Mechanical subsystem

The forces and due to the nonlinear spring ($F_s(t)$) and the damper ($F_d(t)$) are:

$$F_s(t) = K_1 x_1(t) + K_2 x_1^2(t) \;\; ; F_d(t) = b\frac{dx_1(t)}{dt} \;\; ; x_1(t) = x_p(t) - d_1 \tag{1}$$

where $F_s(t)$ and $F_d(t)$ are zero when $x_1(t) = d_1$. The Newton motion equation of the piston as function of the coordinate $x(t)$ referred to the OXY reference system (see Fig 1) can be written as:

$$m\frac{d^2x(t)}{dt^2} = F(t) + K_1\left[x_p(t) - d_1\right] + K_2\left[x_p(t) - d_1\right]^3 + b\frac{d\left[x_p(t) - d_1\right]}{dt} - SP(t) \tag{2}$$

where S is the piston cross section. In accordance with the reference system shown in Fig 1, it is deduced that the gas volume $V(t)$ and the mobile piston displacement $x(t)$ can be written as a function of an effective volume V_e as:

$$\left.\begin{array}{c} L = x(t) + c/2 + x_p(t) \Rightarrow x_p(t) = L - c/2 - x(t) \\ d = L - c/2 \;\; ; \;\; x_p(t) = d - x(t) \;\; ; \;\; x_1(t) = x_p(t) - d_1 \\ V(t) = S \cdot x_p(t) - \left(V_c + V_{sd} + V_a\right) = V_e - S \cdot x(t) \Rightarrow x(t) = \dfrac{V_e - V(t)}{S} \\ V_e = S \cdot d - \left(V_c + V_{sd} + V_a\right) \;\; ; \;\; x_p(t) = d - \left(\dfrac{V_e - V(t)}{S}\right) \end{array}\right\} \tag{3}$$

where $V(t)$ is the gas volume, V_c and V_{sd} are the volumes of the heating coils and the spring-damper respectively, and V_a is a fixed accessible gas volume between the bumpers and the end of the cylinder. It should be noted that $x_p(t)$ and $x_1(t)$ represent the piston position with respect to the end of the cylinder and the bumpers B respectively. Furthermore, the piston motion is limited between $d = L - c/2$ and d_1. According to Eqs (3), Eq (2) can be written in term of the volume $V(t)$ as:

$$-\frac{m}{S}\frac{d^2V(t)}{dt^2}=K_1\left[d-\left(\frac{V_e-V(t)}{S}\right)-d_1\right]+K_2\left[d-\left(\frac{V_e-V(t)}{S}\right)-d_1\right]^3+$$
$$+b\frac{d\left[d-\left(\frac{V_e-V(t)}{S}\right)-d_1\right]}{dt}+F(t)-S\cdot P(t) \tag{4}$$

Introducing the nomenclature:

$$\bar{d}_1=d_1-\left(\frac{V_c+V_{sd}+V_a}{S}\right)\Rightarrow S\left(d_1-\bar{d}_1\right)=V_c+V_{sd}+V_a$$
$$V'(t)=V(t)-V_s\ ;\ V_{se}=V_s-S\cdot\bar{d}_1 \tag{5}$$
$$P'(t)=P(t)-P_s\ ;\ F'(t)=F(t)-F_s$$

where V_s is a steady-state gas volume defined as $V_s=S\cdot x_{pe}$ being x_{pe} an arbitrary piston position with respect to the end of the cylinder (see Fig 1), whereas F_s and P_s are steady-state values for the force and pressure respectively. The model equations (4) and (5) can be simplified assuming that the volumes V_c, V_{sd} and V_a are chosen so that $\bar{d}_1=0$ and thus $V_{se}=V_s$. It should be remarked that the steady-state volume V_s depends on the values for K_1, K_2, F_s and P_s, which are chosen to obtain three equilibrium points for the mobile piston as it will be analyzed later. Substituting equation (5) into Eq (4), the motion equation of the mobile piston can be written as:

$$\frac{d^2V'(t)}{dt^2}=-\frac{K_1}{m}\left[V'(t)+V_{se}\right]-\frac{K_2}{mS^2}\left[V'(t)+V_{se}\right]^3-\frac{b}{m}\frac{dV'(t)}{dt}+$$
$$+\frac{S^2}{m}\left[P'(t)+P_s\right]-\frac{S}{m}\left[F'(t)+F_s\right] \tag{6}$$

Taking into account that the gas may reach a very high pressure, the use of only the spring and damper to balance the piston would require very high values for K_1, K_2 and b, which would lead to prohibitive values for the oscillation frequencies of the piston ($\sim K_1/m$). Consequently, to achieve a large range of pressures as well as the possibility of studying different gas behaviors, it is necessary to ensure that the piston has several equilibrium points. For this purpose, we define the force $F'(t) + F_s$ of Eq (6) by incorporating three terms as follows:

$$\frac{S}{m}\left[F'(t)+F_s\right]=\left\{\begin{array}{c}\frac{S^2}{m}\left[P'(t)+P_s\right]-\frac{K}{S^2}\left[V'(t)+V_{se}\right]^2+\frac{S^2}{m}P_{1s}- \\ -f_p\frac{b}{m}\frac{dV'(t)}{dt}+ \\ +C(t)\left[V'(t)+k_L\right]\frac{dV'(t)}{dt}\end{array}\right\} \tag{7}$$

When Eq (7) is substituted into Eq (6), the first term $\left(S^2/m\right)\left[P'(t)+P_s\right]$ cancels the gas pressure, and the values of K and P_{1s} are chosen in accordance with K_1 and K_2 to obtain three equilibrium points in steady state. In the second term, f_p is a variable factor such that the friction effect is considered when $f_p = 0$ and removed when $f_p = 1$. The third term is formed by a nonlinear function with two adjustable parameters $C(t)$ and k_L -whose meaning will be clarified in the analysis of the chaotic motion-. Substituting Eq (7) into Eq (6) it follows that:

$$\left.\begin{array}{c}\frac{d^2V'(t)}{dt^2}=-\frac{K_1}{m}\left[V'(t)+V_{se}\right]-\frac{K_2}{mS^2}\left[V'(t)+V_{se}\right]^3-\left(1-f_p\right)\frac{dV'(t)}{dt}+ \\ \frac{K}{mS}\left[V'(t)+V_{se}\right]^2+\frac{S^2}{m}P_{1s}+C(t)\left[V'(t)+k_L\right]\frac{dV'(t)}{dt}\end{array}\right\} \tag{8}$$

2.2 Thermal subsystem

Assuming that the mechanical work done on the gas is reversible, the most general expression for the first principle of Thermodynamics is (Annamalai et al., 2002; Hougen et al. 1954):

$$nc_v(t)\frac{dT(t)}{dt}+\left[T\left(\frac{\partial P}{\partial T}\right)_v-P\right]\frac{dV(t)}{dt}=Q(t)+Q_1(t)-P\frac{dV(t)}{dt} \tag{9}$$

where n is the number of gas moles, $c_v(t)$ is the gas specific heat at constant volume, V is the gas volume, $v = V/n$ is the molar volume, P and T are the gas pressure and temperature respectively and $Q(t)$, $Q_1(t)$ are the reversible heat fluxes supplied by the heating coils (see Fig 1). The specific heat at constant volume c_v will be calculated

from the specific heat at constant low pressure $c_p^*(T)$ (which is temperature dependent) as :

$$c_v = c_p^*(T) - R + T\int_{\infty}^{v}\left(\frac{\partial^2 P}{\partial T^2}\right)_v dv \tag{10}$$

where R is the perfect gas constant. The heat flux generated in coil C (see Fig 1) is given by:

$$Q(t) = K_s F_v(t) \;\; ; \quad F_v(t) = K_p\left[T_s - T(t) + \frac{1}{\tau_i}\int_0^t \left[T_s - T(\tau)\right] d\tau\right] \tag{11}$$

where K_s is the heating coil constant. See (Pérez-Molina et al., 2016) for details). The flow rate $F_v(t)$ is defined by means of the equation of a PI controller (Albertos et al., 2004; Pérez_Molina et al., 2016) with proportional constant K_p and reset time τ_i. From Eqs (11) it is deduced that:

$$\frac{dQ(t)}{dt} = -K_p K_s \frac{dT(t)}{dt} + \frac{K_p K_s}{\tau_i}\left[T_s - T(t)\right] \tag{12}$$

Eqs (11) and (12) define the control loop 1 shown in Fig 1. Furthermore, the nonlinear control loop 2 can be defined according to the layout of Fig 1 through the following equations:

$$\left.\begin{aligned} F_{v1}(t) &= f(t)\left[\alpha K_s F_v(t) + \beta\left[T_s - T(t)\right]\right] \\ Q_1(t) &= K_s f(t)\left[\alpha K_s F_v(t) + \beta\left[T_s - T(t)\right]\right] \end{aligned}\right\} \tag{13}$$

where $Q_1(t)$ is the heat flux generated in coil C_1, whereas α and β are constants which are chosen to stabilize the thermal subsystem. Substituting Eq (13) into Eq (9) it is deduced that:

$$\frac{dT(t)}{dt} = \frac{Q(t)}{nc_v(t)} + \frac{K_s f(t)}{nc_v(t)}\left[\alpha Q(t) + \beta\left[T_s - T(t)\right]\right] - \frac{T(t)}{nc_v(t)}\left(\frac{\partial P}{\partial T}\right)_v \frac{dV(t)}{dt} \tag{14}$$

Now we shall define the nonlinear function *f(t)* of Eqs (13) and (14) so that the linear part of the thermal subsystem given by Eqs (12) and (14) has eigenvalues with negative real parts, thus ensuring its stability. For this purpose, *f(t)* is defined as follows:

$$f(t) = c_v(t)\left[1 - \frac{Q_s}{Q(t)}\right] - \frac{Q_s}{\alpha K_s Q(t)} \tag{15}$$

where Q_s is the steady-state value of *Q(t)* and T_s is the desired gas temperature. Substituting Eq (15) into Eq (14) it follows that:

$$\begin{aligned} \frac{dT(t)}{dt} &= \frac{\alpha K_s}{n}\left[Q(t) - Q_s\right] - \frac{\beta K_s}{n}\left[T(t) - T_s\right] + \frac{Q(t) - Q_s}{nc_v(t)} + \\ &+ \frac{\beta}{n}\left[\frac{T(t) - T_s}{Q(T)}\right]\left[K_s + \frac{Q_s}{\alpha c_v(t)}\right] - \frac{T(t)}{nc_v(t)}\left(\frac{\partial P}{\partial T}\right)_v \frac{dV(t)}{dt} \end{aligned} \tag{16}$$

To simplify the system analysis, it is convenient to introduce the variables $T'(t) = T(t) - T_s$; $Q'(t) = Q(t) - Q_s$ so that Eqs (12) and (16) can be rewritten as:

$$\begin{aligned} \frac{dT'(t)}{dt} &= -\frac{\beta K_s}{n}T'(t) + \frac{\alpha K_s}{n}Q'(t) + \frac{Q'(t)}{nc_v(t)} + \left[K_s + \frac{1}{\alpha c_v(t)}\right]\frac{\beta Q_s}{n}\frac{T'(t)}{\left[Q'(t) + Q_s\right]} \\ &- \left[\frac{T'(t) + T_s}{nc_v(t)}\right]\left(\frac{\partial P}{\partial T}\right)_v \frac{dV'(t)}{dt} \end{aligned} \tag{17}$$

$$\frac{dQ'(t)}{dt} = -K_p K_s \frac{dT'(t)}{dt} - \frac{K_p K_s}{\tau_i}T'(t) \tag{18}$$

Eqs (8), (17) and (18) constitute the mathematical model of the system. It should be noticed that the particular choice of *f(t)* given in Eq (15) implies that the system defined by Eqs (17) and (18) has an equilibrium point (T_s, Q_s) which is a stable focus. On the other hand, the PI controller defined by Eqs (11) will keep the gas temperature approximately constant around the set point temperature T_s.

2.3 Equilibrium points of the mechanical and thermal subsystems

In this subsection we shall corroborate that the mechanical subsystem defined by Eq (8) with the parameter values indicated in the legend of Fig 1 has three equilibrium points. Taking into account that $\bar{d}_1 = 0$, the volume *V'(t) + V_{se}* which appears in Eq (8) can be written as:

$$\begin{gathered} V'(t)+V_{se}=V(t)\ ;\ V(t)=S\cdot x_p(t)-(V_c+V_{sd}+V_a) \\ V(t)=S\cdot x_p(t)-S\cdot d_1=S\cdot x_1(t) \end{gathered} \tag{19}$$

The volume $V_p(t)=S\cdot x_1(t)$ can be considered as an accessible volume for the piston, and thus the following deviation variable can be defined:

$$V'(t)+V_{se}=V(t)=V'_p(t)+V_{ps} \tag{20}$$

where V_{ps} is an arbitrary equilibrium volume for the piston referred to the bumpers. Substituting Eq (20) into Eq (8), the equation of the mechanical subsystem can be written in terms of the $V'_p(t)$ variable as follows:

$$\begin{gathered} \frac{d^2V'_p(t)}{dt^2}=-\left(\frac{K_1}{m}+\frac{K_2 3V_{ps}^2}{mS^2}-\frac{K2V_{ps}}{mS}\right)V'_p(t)-\left(\frac{K_2 3V_{ps}}{mS^2}-\frac{K}{mS}\right)V'^2_p(t)-\frac{K_2}{mS^2}V'^3_p(t)+ \\ C(t)\left[V'_p(t)+k_L\right]\frac{dV'_p(t)}{dt}+(f_p-1)\frac{b}{m}\frac{dV'_p(t)}{dt}+\frac{K_2}{mS^2}V_{ps}^3-\frac{K}{mS}V_{ps}^2+\frac{K_1}{m}V_{ps}-\frac{S^2}{m}P_{1s} \end{gathered} \tag{21}$$

The analysis of the equilibrium points and the dynamical properties of the whole mechanical-thermal system are carried out by defining *C(t)* in Eqs (7) and (21) as a harmonic function given by:

$$C(t)=C_0+C_1\sin\omega_L t \tag{22}$$

where C_0, C_1 and ω_L are adjustable parameters. The $V'_p(t)$ volume at an equilibrium point will be zero, and from Eq (21) it is deduced that:

$$y(V_{ps})=\frac{K_2}{mS^2}V_{ps}^3-\frac{K}{mS}V_{ps}^2+\frac{K_1}{m}V_{ps}-\frac{S^2}{m}P_{1s}=0 \tag{23}$$

The values of the constants K_1, K_2, K and P_{1s} have been chosen so that the polynomial given by Eq (23) has three positive roots in order to obtain a piston motion within the cylinder with physically reasonable velocities and frequencies. It should be noticed that the mechanical subsystem is decoupled from the thermal one due to the control force defined by Eq (7), i.e. in Eq (21) the thermal subsystem has no influence on the mechanical one.

In order to analyze the stability of the equilibrium points of the mechanical subsystem, we shall rewrite Eq (21) (taking into account Eq (23)) as a system of two first-order differential equations. For the sake of simplicity in the notation, we first introduce the following parameters:

$$\omega^2 = \left(\frac{K_1}{m} + \frac{3V_{ps}^2 K_2}{mS^2} - \frac{2V_{ps}K}{mS} \right) \; ; \; q = \left(\frac{3V_{ps}K_2}{mS^2} - \frac{K}{mS} \right) \; ; \; r = \frac{K_2}{mS^2} \tag{24}$$

Introducing the variables $z_1'(t) = V_p'(t)$; $z_2'(t) = dV_p'(t)/dt$ and assuming that $C_1 = 0$ and $k_C = 0$, it follows that Eq (21) can be rewritten as:

$$\begin{bmatrix} \dot{z}_1'(t) \\ \dot{z}_2'(t) \end{bmatrix} = \begin{bmatrix} 0 & 1 \\ -\omega^2 & -\left(1-f_p\right)\frac{b}{m} \end{bmatrix} \begin{bmatrix} z_1'(t) \\ z_2'(t) \end{bmatrix} + \begin{bmatrix} 0 \\ -qz_1'^2(t) - rz_1'^3(t) + C_0 z_1'(t) z_2'(t) \end{bmatrix} \tag{25}$$

The eigenvalues of the linear part of Eq (25) are given by:

$$\lambda_{1,2} = -\frac{1}{2}\left(1-f_p\right)\frac{b}{m} \pm \sqrt{\left(\frac{1-f_p}{2}\right)^2 \frac{b^2}{m^2} - \omega^2} \tag{26}$$

On the other hand, the parameter values of Eq (23) are chosen to obtain three equilibrium points P_1, P_2 and P_3, at which the respective slopes m_{P1}, m_{P2} and m_{P3} of the curve $y(V_s)$ (see Fig 2 a)) are:

$$\left.\begin{aligned} m_{P_1} &= \left[\frac{dy(V_{ps})}{dV_s}\right]_{P_1} = \frac{3K_2}{S^2}V_{psP_1}^2 - \frac{2K}{S}V_{psP_1} + K_1 > 0 \\ m_{P_3} &= \left[\frac{dy(V_{ps})}{dV_s}\right]_{P_3} = \frac{3K_2}{S^2}V_{psP_3}^2 - \frac{2K}{S}V_{psP_3} + K_1 > 0 \\ m_{P_2} &= \left[\frac{dy(V_{ps})}{dV_s}\right]_{P_2} = \frac{3K_2}{S^2}V_{psP_2}^2 - \frac{2K}{S}V_{psP_2} + K_1 < 0 \end{aligned}\right\} \quad (27)$$

From the inequalities of Eq (27) it follows that the parameter ω^2 of Eqs (24) and (25) is positive at P_1 and P_3 and negative at P_2. Therefore Eq (25) implies that for $f_p < 1$ a stable focus (node) appears at P_1 and P_3, whereas for $f_p > 1$ an unstable focus (node) appears at P_1 and P_3. It should be noted that $\omega^2 < 0$ at point P_2, and thus an unstable saddle always appears at such point. However, the value $f_p = 1$ leads to a pair of pure complex conjugate eigenvalues or weak focuses at P_1 and P_3, for which the previous conclusions regarding stability cannot be applied, as it will be analyzed in section 3.

The equilibrium points of the thermal subsystem are easier to determine, since the eigenvalues of its linear part are obtained according to Eqs (17) and (18) as:

$$\lambda_{3,4} = -\frac{1}{2}\left(\frac{\beta K_s}{n} + \frac{\alpha K_s^2 K_p}{n}\right) \pm \frac{1}{2}\sqrt{\left(\frac{\beta K_s}{n} + \frac{\alpha K_s^2 K_p}{n}\right)^2 - 4\alpha K_s^2 K_p \frac{\alpha}{n\tau_i}} \quad (28)$$

and thus stability is achieved just by taking:

$$\tau_i < \frac{4n\alpha K_p}{\left(\beta + \alpha K_s K_p\right)^2} \Rightarrow \tau_i = \frac{4n\alpha K_p f_c}{\left(\beta + \alpha K_s K_p\right)^2} \;\; ; \;\; \alpha > 0 \;\; ; \;\; K_p > 0 \;\; ; \;\; f_c < 1 \quad (29)$$

It should be noted that Eq (29) provides an admissible range for the parameters of the temperature PI controller depicted in Fig 1, which is a consequence of the definition of the nonlinear function *f(t)* in Eq (15).

2.4 Numerical simulation procedure

The numerical computations are carried through Eqs (8), (17) and (18) by defining the following state variables:

$$\left[V'(t) \quad dV'(t)/dt \quad T'(t) \quad Q'(t) \quad \omega_L t\right] \equiv \left[x_1(t) \quad x_2(t) \quad x_3(t) \quad x_4(t) \quad x_5(t)\right] \tag{30}$$

where $x_5(t) = \omega_L t$ is an artificial variable to transform the nonautonomous system into an autonomous one with the additional state equation $dx_5(t)/dt = \omega_L$. For the selected values of volume, pressure and temperature, the mole number *n* and the density of a real gas are determined from its state equation. As per Eq (29), for $f_c = 0.001$ the value of the integral action of the PI controller is $\tau_I = 0.1210\ s$.

We shall consider three different simulations for which the initial conditions are defined as follows:

$$\begin{aligned} x_{01} &= \left[-1.01 \cdot V_{se} + Sx_{P_1} \quad 0 \quad f_i T_s \quad 0 \quad 0\right] \\ x_{02} &= \left[-1.01 \cdot V_{se} + Sx_{P_3} \quad 0 \quad f_i T_s \quad 0 \quad 0\right] \\ x_{03} &= \left[f_i V_{se} \quad 0 \quad f_i T_s \quad 0 \quad 0\right] \end{aligned} \tag{31}$$

where f_i is a small value (e.g. $f_i = 0.001$) and T_s is the set temperature, which will be larger than the critical temperature of the gas. The initial conditions x_{01} and x_{02} will be used to investigate the gas behavior around the equilibrium points P_1 and P_3 respectively, whereas x_{03} will be used for an arbitrary initial piston position. It should be remarked that at $t = 0$ the heat fluxes at coils C and C_1 (see Fig 1) are the corresponding steady-state values $Q_s = K_s F_{se}$ and $Q_{s1} = -K_s F_{se}$ (Eqs (13) and (15)) respectively. Next, the following steps are carried out:

a) At $t = 0$ all the deviation state variables given by Eqs (30) are known from the initial conditions given by Eqs (31). The initial values for the pressure P_s, temperature T_s and gas mole number *n* are used to obtain the specific volume from the state equation as well as to assure that the piston position remains

within the limits $d_1 < x_1(t) < L - c/2$ (see Fig 1). Thus, the following values are calculated:

$$\begin{aligned} v(0) &= 1000\left[x_1(0) + V_s\right]/n \;\; ; \;\; x_1(0) = x_1(0) + V_{se}/S \\ T(0) &= x_3(0) + T_s \;\; ; \;\; P(0) = f\left[T(0), v(0)\right] \;\; ; \;\; c_v(0) = f_v\left[T(0), P(0), v(0)\right] \end{aligned} \tag{32}$$

where *f(.)* denotes the gas state equation and $f_v(.)$ represents the calculation of Eq (10).

b) In the next integration step $t = T$, all the state variables are calculated through Runge-Kuta integration method for the model equations (6), (7), (17) and (18). In this step, all the calculations indicated in Eqs (32) must be repeated four times. For the considered state equation, the corresponding specific volume *v(T)* with physical meaning must be found, from which the specific heat at constant volume $c_v(T)$ and other thermodynamic magnitudes such as specific heat at constant pressure $c_p(T)$ and the isothermal compressibility coefficient can be also obtained. The condition $d_1 < x_1(t) < L - c/2$ is fulfilled in all the calculations.

c) The state variables are updated by using the Runge-Kutta formula, and thus the integration process is ready for the following iteration $t = 2T$.

Figs 2 b), c) and d) show two simulations by using the Soave-Redlich-Kwong (SRK) state equation for the nitrogen as real gas (see Appendix) taking $f_p = 1$ (so that P_1 and P_3 are weak focuses), $C_0 = -500$, $C_1 = 0$, $k_L = 0$ and assuming that the initial conditions are close to the equilibrium point P_3 (see Fig 2 a)). It should be noted that the weak focus P_3 of Fig 2 b) is unstable, and at $t \approx 45$ *s* the piston position jumps to the other weak focus P_1 remaining around this point, that appears to be stable. Fig 2 c) shows the effect of the PI controller defined by Eq (11), where the gas clearly shows an almost isotherm behavior with small oscillations around the set temperature $T_s = 300$ *K*. Fig 2 d) also shows the oscillation of the heat flux transmitted by coils C and C_1 (see Fig 1) around the steady state value obtained from Eqs (11).

Figure 2

An interesting result is shown in Fig 3 a), where the gas pressure varies abruptly from the initial pressure $P_s = 50\ atm$ (when the piston is oscillating around the weak focus P_3) to a maximum value of *203 atm*. Furthermore, a steady-state pressure of *141 atm* is reached when the piston remains oscillating around the weak focus P_1 with an almost constant gas temperature (see Fig 2 c)) and the specific gas volume varying as shows in Fig 3 b). In Fig 3 c) the phase portrait of the piston position is plotted, thus corroborating that the weak focuses P_3 and P_1 are unstable and stable respectively. Fig 3 d) also shows the compressibility factor. The relevance of the previously defined model and control laws relies on the possibility of investigating different state equations through the virial coefficients obtained from the simulation results.

Figure 3

3. Analysis of the chaotic behavior through the first Lyapunov value

In this section we shall investigate a procedure to obtain chaotic behavior for the gas pressures and volumes while keeping the gas temperature almost constant with small oscillations around the set point. It should be noticed that the almost isothermal chaotic data obtained from the device of Fig 1 must involve great excursions for the gas pressures and volumes to correctly estimate the virial coefficients for different state equations. Due to the decoupling between the mechanical and thermal subsystems (as discussed in the previous section), only the mechanical subsystem given by Eq (24) will be considered assuming that $f_p = 1$, so that points P_1 and P_3 of Fig 2 a) are weak focuses.

It is well known that the stability of a weak focus depends on the sign of the first Lyapunov value (Guckenheimer et al., 1983; Wiggins, 2000; Pérez_Polo et al., 2014), which is calculated through the normal form of Eqs (24). For this purpose, we obtain the Jordan canonical form of Eq (24) by means of the eigenvector associated to the eigenvalue $+i\omega$ to obtain the transformation matrix P_t, which defines a coordinate transformation as:

$$P_t = \begin{bmatrix} 1 & 0 \\ 0 & \omega \end{bmatrix} \Rightarrow P_t^{-1} = \frac{1}{\omega}\begin{bmatrix} \omega & 0 \\ 0 & 1 \end{bmatrix} \Rightarrow \begin{bmatrix} z_1'(t) \\ z_2'(t) \end{bmatrix} = P_t \begin{bmatrix} x(t) \\ y(t) \end{bmatrix} \tag{33}$$

Substituting Eq (33) into Eq (25) we obtain the normal form of the mechanical subsystem as follows:

$$\begin{bmatrix} \dot{x}(t) \\ \dot{y}(t) \end{bmatrix} = \begin{bmatrix} 0 & \omega \\ -\omega & 0 \end{bmatrix} \begin{bmatrix} x(t) \\ y(t) \end{bmatrix} + \begin{bmatrix} 0 \\ -(q/\omega)x(t)^2 - (r/\omega)x(t)^3 + C_0 x(t) y(t) \end{bmatrix} \tag{34}$$

Introducing the notation:

$$f^1\left[x(t), y(t)\right] = 0 \;;\; f^2\left[x(t), y(t)\right] = -(q/\omega)x(t)^2 - (r/\omega)x(t)^3 + C_0 x(t) y(t) \tag{35}$$

the first Lyapunov value can be calculated as:

$$\begin{aligned} L_1 = \frac{1}{16}\left[f^1_{xxx} + f^1_{xyy} + f^2_{xxy} + f^2_{yyy} \right] + \\ + \frac{1}{16\omega}\left[f^1_{xy}\left(f^1_{xx} + f^1_{yy} \right) - f^2_{xy}\left(f^2_{xx} + f^2_{yy} \right) - f^1_{xx} f^2_{xx} + f^1_{yy} f^2_{yy} \right] \end{aligned} \tag{36}$$

where the subscripts denote partial derivatives (i.e. $f^1_{xxx} = \partial^3 f^1 / \partial x^3$ and so on). All the partial derivatives are calculated at the bifurcation point, which is the origin (0,0) since we are using deviation variables as per Eqs (25). Once the first Lyapunov value L_1 has been calculated, if $L_1 > 0$ then the weak focus is unstable, and conversely if $L_1 < 0$ then we have a stable weak focus. From Eqs (35) and (36) it is deduced that the first Lyapunov value is a constant, i.e.:

$$L_1 = -\frac{C_0 q}{8\omega} \tag{37}$$

From Eq (37) it follows that when $q > 0$ we must choose $C_0 > 0$ to obtain a stable weak focus and $C_0 < 0$ to obtain an unstable weak focus. Although the stability of a weak focus is solely determined by the sign of L_1, if we choose a large value for C_0 then the damping will quickly decrease when moving away from the equilibrium point

and vice-versa. The previous considerations explain the behavior shown in Fig 2 b), where according to the parameter values indicated at the legend of Fig 1 the values of q and ω at point P_3 are $q_{P_3} = 3.7020 \cdot 10^4 > 0$ and $\omega_{P_3} = 6.9780$ rad/s . Thus taking C_0 = *-500* it is clear that the first Lyapunov value L_1 is positive at P_3, which is thus an unstable weak focus. Similarly, at point P_1 we have that $q_{P_1} = -3.8683 \cdot 10^4 < 0$ and $\omega_{P_1} = 7.4540$ rad/s , so $L_1 < 0$ and thus P_1 is a stable weak focus.

It should be remarked that taking $C(t) = 0$ in Eq (7) would have implied that $L_1 = 0$, thus making it impossible to determine the stability of the weak focuses P_1 and P_3. This justifies the choice of the third term of Eq (7), and taking into account the value of $C(t)$ given in Eq (22) the first Lyapunov value takes the form:

$$L_1(t) = -\frac{q\left(C_0 + C_1 \sin \omega_L t\right)}{8\omega} \tag{38}$$

Taking $C_0 = 0$ and taking into account Eq (22), the linear part of Eqs (25) remains unaltered whereas the nonlinear part changes to:

$$-qz_1'^2(t) - rz_1'^3(t) + C_1 \sin x_5(t)\left[z_1'(t) + k_C\right] z_2'(t) \tag{39}$$

and thus the equilibrium points P_1, P_2 and P_3 have the same properties as the ones analyzed in the previous section. Since the piston has only two possible equilibrium points (P_1 and P_3), it will jump between P_1 and P_3 with large oscillations in the gas pressure and an almost constant temperature (recall Eqs (17) and (18) for the thermal subsystem). This feature provides a potential route for chaotic behavior in the system. It should be remarked that there is no currently a definitive criterion for the appearance of chaotic behavior, and thus we will use the sensitive dependence, the Lyapunov exponents and the power spectral density to argue that the system behavior is chaotic for some values of C_1 and ω_L in Eq (22).

Fig 4 shows the results of two simulations by using the SRK state equation and methane as real gas. In such simulations, Eqs (8), (17), (18), (22) and (30) have been

used taking $k_L = Sd_1$ and assuming that the initial conditions x_{30} of Eqs (31) with $f_i = 0.001$ differ in 10^{-5} at $t = 0$. Furthermore, the first Lyapunov value has been harmonically varied in accordance with Eq (38) taking $C_0 = 0$, $C_1 = -500$ and $\omega_L = 35$ *rad/s*. Fig 4 a) shows that the gas pressures are completely different at approximately $t = 200$ *s* and thus the system has sensitive dependence, which is corroborated in Fig 4 b) by plotting the error of the gas pressure as a function of the time.

The gas temperatures in Fig 4 c) also show sensitive dependence, although due to the effect of the PI controller both temperatures remain almost constant with small oscillations around the set point $T_s = 500$ *K*. It should be remarked that the gas pressure exhibits great excursions, which will be used for the estimation of virial coefficients. Fig 4 d) shows that the piston positions have also sensitive dependence, which is manifested as a great difference between $x_p(t)$ and $x_{pd}(t)$ when the piston jumps between the equilibrium points P_1 and P_3.

Figure 4

Fig 5 a) shows two strange attractors in the phase plane $x_p(t)$-$dx_p(t)/dt$ with the same sensitive dependence as in Fig 4, and the chaotic behavior as well as the limitation in the left side of the attractors due to the bumpers (see Fig 1) can be appreciated. On the other hand, Fig 5 b) shows a simulation of the piston position up to a time of 800 s with $C_1 = -1000$. Unlike Fig 4, in this case it is clear that the piston jumps regularly between P_1 and P_3 and thus the movement is periodic. In Fig 5 c) the phase portrait $x_p(t)$-$dx_p(t)/dt$ has been plotted, thus corroborating the periodicity.

Figure 5

The chaotic oscillations shown in Figs 4 and 5 a) are also corroborated by calculating all Lyapunov exponents of the system according to Eqs (8), (17), (18), (22) and (30). The components of the vector field associated to the system equations can then be written as:

$$
\left.
\begin{aligned}
f_1 &= \frac{dx_1(t)}{dt} = x_2(t) \\
f_2 &= -\frac{K_1}{m}\left[x_1(t)+V_{se}\right] - \frac{K_2}{mS^2}\left[x_1(t)+V_{se}\right]^3 - \left(1-f_p\right)\frac{b}{m}x_2(t) + \frac{K}{mS}\left[x_1(t)+V_{se}\right]^2 + \\
&\quad + C_1 \sin x_5(t)\left[x_1(t)+Sd_1\right]x_2(t) \\
f_3 &= -\frac{\beta K_s}{n}x_3(t) + \frac{\alpha K_s}{n}x_4(t) + \left[K_s + \frac{1}{\alpha c_v(t)}\right]\frac{\beta Q_s x_3(t)}{n\left[x_4(t)+Q_s\right]} + \\
&\frac{x_4(t)}{nc_v(t)} - \left[\frac{x_3(t)+T_s}{nc_v(t)}\right]\left(\frac{\partial P}{\partial T}\right)_v x_2(t) \quad ; \quad f_4 = -K_s K_p f_3 - \frac{K_s K_p}{\tau_i}x_3 \quad ; \quad f_5 = \omega_L
\end{aligned}
\right\} \quad (40)
$$

Linearizing the vector field of Eqs (40) along a trajectory and applying the Gram-Smidth orthogonalization method (Pérez-Polo et al., 2014; Lichtenberg et al., 1992; Pérez-Polo et al., 2007), the Lyapunov exponents are obtained as function of time as shown in Fig 6 a). In particular, the whole set of Lyapunov exponents at t = 400 s is given by (Benettin et al., part I-part II 1980):

$$
L_1 = \left[0.11951368 \quad 0.00935840 \quad -0.0050379306 \quad -0.107759160 \quad 0\right] \quad (41)
$$

Equation (41) shows that there are two positive exponents (hyperchaotic system) which are associated to the mechanical and thermal subsystems. This result is another indicator that the oscillations of Figs 4 and 5 a) are chaotic.

Fig 6 b) shows the sum of the Lyapunov exponents together with the divergence of the vector field given by Eqs (40). The sum of Lyapunov exponents is 0.01508479 whereas the mean value of the vector field divergence is 0.015084482, and thus the following approximation is fulfilled (Guckenheimer at al. 1983; Lichtenberg et al. 1992; Wiggins, 2000):

$$
\sum_{i=1}^{5} LY_i \approx div\overline{f} \quad (42)
$$

Eq (42) constitutes an indirect verification for the correctness of the numerical computations. In Fig 6 c), the calculated power spectral density for the gas volume as a

function of the time shows a broadband spectrum with decreasing oscillations, which is a characteristic feature of a chaotic signal (Lichtenberg et al., 1992). In addition, the zone of low frequencies has been enlarged to show that the applied external disturbance of $\omega_L = 2\pi/TC = 2\pi/35 = 0.1795\ rad/s$ clearly appears within the spectrum. Fig 6 d) shows the specific heats at constant volume $c_v(t)$ and constant pressure $c_p(t)$ calculated through the SRK state equation (Eq (A2)), where $c_p^*(t)$ in Eq (10) is defined as a function of the temperature given by:

$$c_p^*(t) = A + BT(t) + CT^2(t) + DT^3(t) + ET^4(t) \tag{43}$$

being $T(t)$ is the gas temperature (Yaws, 1999). Once $c_v(t)$ is known, $c_p(t)$ is calculated from the coefficients of isobaric expansion and isothermal compressibility (Annamalai et al., 2002; Hougen et al. 1954). It should be remarked that the abrupt changes in $c_v(t)$ and $c_p(t)$ are due to the chaotic oscillations, whereas the thermodynamic inequality $c_p(t) > c_v(t)$ is always fulfilled. Finally, it must be taken into account that we have used the SRK state equation since it provides the smallest error compared to the state equation of high precision, as we will see in the next sections.

Figure 6

It should be remarked that our model relies on concentrated parameters and that the chaotic behavior appears in the supercritical zone (above the critical point) of the gas. An example of model based on partial differential equations which takes into account trans-critical phenomena with the appearance of chaos can be found in Chen et al., 2012.

4. Real gas in chaotic regime for different state equations and virial coefficients

In this section we shall consider the volumetric and caloric properties of some cubic and non-cubic state equations, and how these properties are related to the behavior of several non-polar real gases when they are in chaotic regime as it was analyzed in section 3.

4.1 Cubic state equations

The general expression for a cubic state equation can be written as (Poling et al. 2001):

$$z = \frac{Pv}{RT} = \frac{v}{v-b} - \frac{\left[\Theta(T)/RT\right]v(v-\eta)}{(v-b)\left(v^2+\delta_1 v+\varepsilon\right)} \tag{44}$$

where $\Theta(T)$, η, δ_1 and ε depend on the particular state equation, as shown in the Appendix. According to Eq (44), the general volumetric equation is given by:

$$v^3 + \left(\delta_1 - b - \frac{RT}{P}\right)v^2 + \left(\varepsilon - b\delta_1 - \frac{\delta_1 RT}{P} + \frac{\Theta(T)}{P}\right)v - \frac{\Theta(T)\eta}{P} - b\varepsilon - \frac{\varepsilon RT}{P} = 0 \tag{45}$$

For the state equations considered in this work we assume that $\eta = b$ and that the roots of Eq (45) provide the specific volume as a function of the gas temperature and pressure. Since we consider temperatures above the critical one, Eq (45) has two complex conjugates roots and one real root which will be the sought specific volume of the gas. In all calculations, the following equilibrium thermodynamic condition is fulfilled (Annamalai et al., 2002; Hougen et al., 1954):

$$\left(\frac{\partial v}{\partial T}\right)_P \left(\frac{\partial T}{\partial P}\right)_v \left(\frac{\partial P}{\partial v}\right)_T = -1 \tag{46}$$

As per Eq (44), the isobaric expansion coefficient can be obtained as $\beta_c = (1/v)(\partial v/\partial T)_P$, whereas the isothermal compressibility coefficient is given by $\kappa_c = -(1/v)(\partial v/\partial P)_T$. The specific heats at constant volume and pressure are deduced from Eqs (10) and (44), which lead to the following general expressions (Mason et al., 1968; Annamalai et al., 2002; Poling et al., 2001; Tassios, 1993; Hougen et al. 1954):

$$c_v = c_p^* - R - T\frac{\partial^2 \Theta}{\partial T^2}\int_{\infty}^{v}\frac{dv}{v^2+\delta_1 v+\varepsilon} \quad ; \quad c_p - c_v = \frac{Tv\beta_c^2}{\kappa_c} \tag{47}$$

4.2 Non cubic state equations

As non cubic state equations, we will consider the Beattie-Bridgeman (BB) equation, the empirical high precision (HP) state equation and the viral equations (Span, 2000; Gmehling et al. 2012). The corresponding volumetric equation for the BB state equation is a fourth order equation of the form:

$$\begin{aligned} &v^4-(\alpha_2/P)v^3-(\beta_2/P)v^2-(\gamma_2/P)v-(\delta_2/P)=0 \\ &\alpha_2=RT \quad ; \quad \beta_2=-A_0+B_0RT-cR/T^2 \\ &\gamma_2=aA_0-bB_0RT-cB_0R/T^2 \quad ; \quad \delta_2=bcB_0R/T^2 \end{aligned} \tag{48}$$

where A_0, a, B_0, b and c are constants of the considered real gas. For temperatures above the critical one, Eq (49) has two real roots among which only the largest has physical significance, whereas the other two roots are complex conjugate. From Eqs (48), the corresponding expressions for the specific heat at constant volume can be written as:

$$c_v=c_p^*-R-\frac{6cR}{T^3}\int_{\infty}^{v}\left(-\frac{1}{v^2}-\frac{B_0}{v^3}+\frac{bB_0}{v^4}\right)dv \quad ; \quad c_p-c_v=\frac{Tv\beta_c^2}{\kappa_c} \tag{49}$$

where the values of c_p at low pressures are taken from (Yaws, 1999). The empirical high precision state equation (HP) is defined as a function of the molar Hemlholtz energy, which is written as an ideal part plus a residual part due to the gas non-ideality as follows (Span, 2000; Gmehling et al. 2012):

$$\frac{a(T,\rho)}{RT}=\frac{a^{id}(T,\rho)+a^{R}(T,\rho)}{RT}=\alpha^{id}(T,\rho)+\alpha^{R}(T,\rho) \tag{50}$$

where the superscripts *id* and *R* refer to the ideal and residual parts respectively. The ideal part is defined as:

$$\alpha^{id}(T,\rho)=\frac{1}{RT}\int_{T_0}^{T}c_v^{id}(T)dT-\frac{1}{R}\int_{T_0}^{T}c_v^{id}(T)\frac{dT}{T}+\ln\frac{\rho}{\rho_0}+\frac{a(T_0,\rho_0)}{RT} \tag{51}$$

where T_0 and ρ_0 are reference values for which the gas behavior can be considered to be ideal. The gas pressure and the residual part can be determined for some nonpolar gases according to the following expressions:

$$P(T,\rho) = -\left(\frac{\partial a(T,\rho)}{\partial v}\right)_T$$

$$FP = P(T,\rho) - \rho RT\left[1+\delta\left(\frac{\partial \alpha^R(\tau,\delta)}{\partial\delta}\right)_\tau\right] = 0 \;\; ; \;\; \delta = \frac{\rho}{\rho_c} \;\; ; \;\; \tau = \frac{T_c}{T}$$

$$\begin{aligned}\alpha^R(\tau,\delta) = {} & n_1\delta\tau^{0.25} + n_2\delta\tau^{1.125} + n_3\delta\tau^{1.5} + n_4\delta^2\tau^{1.375} + n_5\delta^3\tau^{0.25} + \\ & n_6\delta^7\tau^{0.875} + n_7\delta^2\tau^{0.625}\exp(-\delta) + n_8\delta^5\tau^{1.75}\exp(-\delta) + n_9\delta\tau^{3.625}\exp(-\delta^2) + \\ & n_{10}\delta^4\tau^{3.625}\exp(-\delta^2) + n_{11}\delta^3\tau^{14.5}\exp(-\delta^3) + n_{12}\delta^4\tau^{12}\exp(-\delta^3)\end{aligned} \tag{52}$$

where ρ_c and T_c are the critical density and the critical temperature respectively, whereas n_i *(i = 1,...,12)* are empirical constants which are tabulated for each real gas. In this context, it is clear that obtaining relations similar to the ones of Eq (45) or (49) is not feasible. However, for each temperature *T* and pressure *P* it is possible obtain *FP* in Eq (52) as a function of the specific volume, so that for *FP = 0* we obtain the corresponding specific volume. Taking into account the expression for *P(T,ρ)* in Eq (52) and differentiating at constant pressure and at constant temperature, the isobaric expansion coefficient and the isothermal compressibility coefficient can be respectively determined.

On the other hand, taking into account the thermodynamic relations for the molar Hemlholtz energy, the specific heat at constant volume can be deduced from Eqs (51) and (52). Consequently, similar expressions to the ones of Eqs (47) and (49) can be obtained as follows:

$$c_v(T,\rho) = -R\tau^2\left[\left(\frac{\partial^2\alpha^{id}}{\partial\tau^2}\right)_\delta + \left(\frac{\partial^2\alpha^R(T,\rho)}{\partial\tau^2}\right)\right]$$

$$c_p(T,\rho) - c_v(T,\rho) = R\,\frac{\left[1+\left(\frac{\partial\alpha^R(T,\rho)}{\partial\delta}\right)_\tau - \delta\tau\left(\frac{\partial^2\alpha^R(T,\rho)}{\partial\tau\partial\delta}\right)\right]^2}{\left[1+2\delta\left(\frac{\partial\alpha^R(T,\rho)}{\partial\delta}\right)_\tau - \delta^2\left(\frac{\partial^2\alpha^R(T,\rho)}{\partial\delta^2}\right)\right]} \tag{53}$$

The virial equation with n coefficients is written as:

$$z = \frac{Pv}{RT} = 1 + \frac{C_1(T)}{v} + \frac{C_2(T)}{v^2} + ... + \frac{C_n(T)}{v^n} + ... \tag{54}$$

where $C_i(T)$ $(i = 1,...,n)$ are the temperature dependent virial coefficients (it should be remarked that the virial coefficients are sometimes denoted as $C_1 \equiv B$, $C_2 \equiv C$, $C_3 \equiv D$, $C_4 \equiv E$ and so on). Eq (54) allows to obtain a polynomial as a function of v whose degree depends on the number of virial coefficients, and its largest positive root is the specific volume with physical meaning. By calculating $\left(\partial^2 P/\partial T^2\right)_v$ and recalling Eq (10) it follows that:

$$c_v = c_p^* - R - RT\sum_{i=1}^{n}\left(2\frac{dC_i(T)}{dT} + T\frac{d^2C_i(T)}{dT^2}\right)\left(\frac{1}{i\cdot v^i}\right) \quad ; \quad c_p - c_v = \frac{Tv\beta_c^2}{\kappa_c} \tag{55}$$

As in the previous state equations, the value of the specific heat at constant pressure can be determined from the values of β and κ.

It should be remarked that in this paper we consider pressures between 30 atm and 2000 atm as well as temperatures between 250 K and 750 K in all cases (far above the critical point), for which Eqs (47), (49), (52), (53) and (55) are fulfilled. Besides, the control system keeps the gas with an almost constant temperature. Consequently, the state equations provide a reasonably good approximation for the gas behavior even at high pressures.

4.3 Analysis of the required number of virial coefficients for a given temperature

From the previous considerations and the gas chaotic behavior examined in section 3, we shall investigate how the virial coefficients for different real gases can be estimated. Since only the second C_1 (B) and third C_2 (C) virial coefficients are experimentally known with a reasonable accurateness (Dymond et al. 1980; Dymond, et al., 2002), the estimation of higher order coefficients is an important issue to investigate the behavior of a real gas at high pressures (Holleran, 2007; Meng et al., 2004; Elliot et al. 1985; Belanger et al., 1994). It must be emphasized that the device of Fig 1 allows to

reach very high pressures as it appears in Fig 4 a), so we want to analyze the required number of virial coefficients to obtain the compressibility factor *z* given in Eq (54) and depicted in Fig 3 d).

Once the chaotic data for the pressure *P(t)*, temperature *T(t)* and specific volume *v(t)* are known, Eq (54) is rewritten as:

$$y = v\left(\frac{Pv}{RT} - 1\right) = C_1(T) + \frac{C_2(T)}{v} + \frac{C_3(T)}{v^2} + ... + \frac{C_n(T)}{v^{n-1}} \tag{56}$$

Therefore, by adjusting the simulation data as a function of the gas density *(x = ρ = 1/v)* through the left hand term of Eq (56) with the least square polynomial of degree *n – 1*, the virial coefficients can be estimated. It is very important to remark that this procedure provides accurate values only if the gas behavior is almost isotherm, as it was discussed in section 3.

Since only the coefficients *B* and *C* are sufficient to represent the gas behavior at low pressures, a great excursion in the gas pressure values is necessary to investigate the effect of the virial higher order coefficients on the gas properties. For this purpose, the system has been numerically solved with some state equations considering an initial pressure of $P_s = 100\ atm$ and two initial temperatures of $T_s = 300$ and $T_s = 700\ K$ for the argon gas, whose virial coefficients deduced from interpolation of a set of experimental data are (Dymond et al. 1980; Dymond, et al., 2002): $B_{300} = -1.52.10^{-2}$ *liter/mole,* $C_{300} = 1.080.10^{-3}$ *(liter/mol)*^{2}, $B_{700} = 1.51.10^{-2}$ *liter/mole* and $C_{700} = 0.6044.10^{-3}$ *(liter/mol)*^{2}. Fig 7 shows the results of four simulations, where the Redlich-Kwong (RK) state equation has been selected due to the great excursion pressure that it provides. A comparative analysis of all the state equations used in this work will be presented in the next section.

Figure 7

By applying Eq (56) to the simulation data obtained from the RK state equation, the first five virial coefficients are obtained as follows:

$$\begin{gathered}\left[C_1 \quad C_2 \quad C_3 \quad C_4 \quad C_5\right]_{T_s=300} \equiv \\ \equiv\left[-1.5965\cdot10^{-2} \quad 1.0154\cdot10^{-3} \quad 3.9205\cdot10^{-5} \quad -2.3442\cdot10^{-6} \quad 6.7358\cdot10^{-8}\right] \\ \left[C_1 \quad C_2 \quad C_3 \quad C_4 \quad C_5\right]_{T_s=700} \equiv \\ \equiv\left[1.1089\cdot10^{-2} \quad 0.7116\cdot10^{-3} \quad 0.6644\cdot10^{-5} \quad 0.2031\cdot10^{-6} \quad 1.0544\cdot10^{-8}\right]\end{gathered} \tag{57}$$

where each coefficient C_i is expressed in *(liter/mole)*^{i}. According to the previous results, the values of C_1 = B and C_2 = C are in good agreement with the experimental values B_{300} and C_{300} for $T_s = 300\ K$, whereas the discrepancies for $T_s = 700\ K$ (B_{700} and C_{700}) are more remarkable.

In Figs 8 a) and b), the specific volume and temperature are plotted for the initial conditions $P_s = 100\ atm$ and $T_s = 300\ K$. It should be noted that the specific volume remains oscillating between the two weak focuses shown in Figs 2 a) and b), whereas the gas temperature remains almost constant with very small oscillations around the set point. Fig 8 c) shows an attractor in the phase plane for the piston force-velocity $F(t)$-dx_p/dt, where the presence of the weak focuses P_1 and P_3 as well as phase trajectories suggesting a chaotic behavior can be corroborated.

Figure 8

In Fig 9 a), Eq (56) has been plotted by using the simulation values indicated in Figs 7a), 8 a) and 8 b) as a function of the gas density ρ, where the value of the first virial coefficient can be determined when $\rho \rightarrow 0$. In this case, the points marked with asterisk are the values deduced from Eq (56) taking $n = 5$ (fifth degree polynomial). In addition, the simulation results are marked with dots that exhibit a chaotic pattern within a zone which is very tiny due to the almost isotherm gas behavior. Fig 9 b) shows the compressibility coefficients z_B, z_{BC} and z_{BCD} obtained through one, two and three virial coefficients respectively, and assuming the numerical values taken from Eq (57) for $T_s = 300\ K$. It should be noted that the difference between z_{BC} and z_{BCD} is very small for pressures below approximately 600 atm.

Figure 9

The effect of the number of virial coefficients on the gas behavior is corroborated in Fig 10. Fig 10 a) shows the plots of z_{BC} and z_{BCDE} for the values indicated in Eq (57) for $T_s = 300\ K$ and the value of $z_s = P(t)v(t)/R.T(t)$ deduced from the chaotic data of Figs 7 and 8. It is clear that at high pressures only four virial coefficients could be sufficient to obtain the compressibility coefficient with adequate precision. To corroborate the previous assertion, Fig 10 b) shows the values of z_a deduced from Eq (54) and assuming five virial coefficients in Eq (57). In Figs 10 c) and d), the errors in the compressibility coefficient clearly show the ranges of pressure for which a certain number of virial coefficients must be chosen.

Figure 10

4.4 Analysis of the number of virial coefficients required for a set of predetermined temperatures

Once the virial coefficients for the RK state equation have been determined from the chaotic simulation data, we shall study the accurateness of the state equations (Eqs (44) and (48)) as a function of the chosen number of virial coefficients by taking the high precision state equation (Eq (52)) as reference. For this purpose, a set of temperatures and an initial pressure P_s will be used to estimate the dependence of the virial coefficients with temperature.

It should be taken into account that the piston position is limited by the bumpers (see Fig 1) and thus the gas mole number cannot be chosen arbitrarily, since negative pressures without physical meaning might appear. To avoid this problem we shall analyze the high precision state equation given by Eqs (52), although the same considerations would apply for any of the previously considered state equations. The following steps have been considered:

i) We choose an admissible set of specific volumes. The parameter b_1 of the SRK state equation (see Appendix), which is defined as function of the critical properties of a particular gas, can be adequate as a reference value. For example:

$$v_{\min}^{initial} = 2b_1 \;\; ; \;\; v_{\max}^{initial} = 1000b_1 \Rightarrow v^{initial} = \left[v_{\min}^{initial} \quad . \quad . \quad . \quad v_{\max}^{initial} \right] \tag{58}$$

ii) From Eq (58), the densities and the parameter δ of Eq (52) are determined as follows:

$$\rho^{initial} = \left[\rho_{\min}^{initial} = 1/v_{\max}^{initial} \quad . \quad . \quad . \quad \rho_{\max}^{initial} = 1/v_{\min}^{initial} \right] \;\; ; \;\; \delta^{initial} = v_c / v^{initial} \tag{59}$$

iii) We define a set of temperatures $T = \left[T_1 \quad T_2 \quad . \quad . \quad T_n \right]$ and a pressure P_s, so that for each temperature T_j the following function is obtained:

$$FP = P_s - \rho^{initial} R T_j \left[1 + \delta^{initial} \left(\frac{\partial \alpha^R \left(\tau_j, \delta \right)}{\partial \delta} \right)_{\tau_j} \right] \tag{60}$$

The value *FP = 0* leads to the density value $\delta_j^{initial}$ and the corresponding specific volume $v_j = v_c / \delta_j^{initial}$.

iv) From the value of v_j and the gas volume V_s, the mole number $n_j = V_s / v_j$ can be obtained for an arbitrary piston position. It should be noted that the integral action of the temperature PI controller can now be calculated through Eq (29).

v) Since the piston position is limited, the minimum specific gas volume for the gas volume $S.d_1$ will be $v_j^{\min} = Sd_1 / n_j$. With this minimum specific volume, the gas pressure is calculated again. If the obtained gas pressure is negative or takes too high values, steps iii) to v) are repeated with a smaller value for P_s.

The previous steps for the PR and HP state equations have been applied for the oxygen taking 11 temperatures in the range 200-650 K with an initial pressure of 20 atm. To obtain chaotic behavior, the same parameter values of the section 3 are used. In Fig 11 a), the pressures obtained with the PR state equation are plotted, and similar results for the HP state equation are obtained. In Fig 11 b), the corresponding specific

volumes for the HP state equation are plotted. It can be corroborated that all pressures and specific volumes have physically meaningful values.

Figs 11 c) and d) show the virial coefficients obtained through the PR and HP state equations. To corroborate the calculations for each state equation, the virial coefficients C_i are calculated by introducing the chaotic simulation data into Eq (56), thus obtaining x_1 and y_1, which are adjusted by the least square polynomial to obtain the values marked in the figure as PR_1 and HP_1. On the other hand, with the specific volume and temperatures obtained in the simulation, the gas pressure is calculated from the state equation and thus x_2, y_2 are obtained from Eq (56), for which the corresponding virial coefficients are marked as PR_2 and HP_2. As expected, an exact concordance is obtained.

The experimental data for the coefficients B and C are also plotted in Fig 11. It should be noted that the values of the first virial coefficient for the HP state equation are almost coincident with the experimental data regardless the number of estimated virial coefficients. Furthermore, the second coefficient is also in good agreement with the experimental data when two virial coefficients are adjusted, but it presents a larger discrepancy when three or more viral coefficients are adjusted as shown in Fig 11 d). This tendency has been corroborated for methane, nitrogen, argon and oxygen.

Figure 11

Fig 12 shows the plots of the virial coefficients C_3 to C_6 for the PR and HP state equations. It should be emphasized that the concordance between the results for the PR and HP state equations decreases when the initial pressure increases, which is due to the fact that the HP state equation is more accurate than the PR state equation at high pressures. Similar results have been found for the RK, SRK, PRt, and VDWt state equations. However, the behavior of the BB state equation is slightly different, since it is more difficult to obtain chaotic oscillations by varying the first Lyapunov value.

Figure 12

For a given temperature, the results of Figs 11 and 12 can be used to investigate the pressure range within which a state equation can be compared with the HP state

equation as a function of the number of virial coefficients. It should be recalled that the PI controller maintains the gas temperature almost constant (Albertos et al., 2004; Pérez-Molina et al., 2016), as shown in Figs 2 c), 4 c) and 8 b). In Figs 13 and 14, the pressure error for the high precision (EHP), Peng-Robinson (EPR) Soave-Rechlich-Kwong (ESRK) and volume translated Van der Walls (EVDWt) state equations are defined as follows:

$$EHP = 100 \cdot \left| \frac{P_{HP} - P_{HP}^{ncv}}{P_{HP}} \right| \% \; ; \; EPR = 100 \cdot \left| \frac{P_{PR} - P_{PR}^{ncv}}{P_{PR}} \right| \%$$
$$ESRK = 100 \cdot \left| \frac{P_{SRK} - P_{SRK}^{ncv}}{P_{SRK}} \right| \% \; ; \; EVDWt = 100 \cdot \left| \frac{P_{VDWt} - P_{VDWt}^{ncv}}{P_{VDWt}} \right| \% \tag{61}$$

where P_{HP}, P_{PR}, P_{SRK} and P_{VDWt} are the respective pressures, and the superscript *ncv* indicates the number of virial coefficients.

Figs 13 a) and b) show the relative pressure errors for the oxygen defined by Eq (61). It can be observed that with only two virial coefficients calculated from the chaotic data, the error of the PR state equation is higher than in the HP state equation. However, Fig 13 b) shows that for *ncv = 6* the pressure errors are small for the PR state equation and negligible for the HP state equation. Figs 13 c) and d) show the relative pressure errors for the methane defined by Eqs (61). For an initial pressure P_s of 80 atm the excursion pressure is very high for *ncv = 2*. It should be noted that there is a range of pressures for which the HP state equation has a larger error than the SRK state equation, which can be regarded as an unexpected result. On the other hand, fig 13 d) shows that for *ncv = 6* the error of the HP state equation is negligible for all pressures, but the SRK state equation is accurate only at relatively low pressures.

Figure 13

The relative pressure errors calculated for the nitrogen are shown in Figs 14 a) and b). In this case, the RK state equation is not accurate (except for a very small range of pressures) even for *ncv = 6* virial coefficients, but the relative pressure error for the HP state equation is negligible. On the other hand, Fig 14 b) shows that both the VDWt and HP state equations exhibit an admissible relative error. Furthermore, it should be

noted that the zoom of a small zone clearly shows that the pressures are chaotic within a narrow temperature range around T_s = 250 K. Fig 14 c) shows the range of the chosen temperatures for the VDWt state equation used in the simulation of Fig 14 b), for which the PI controller maintains all the temperatures approximately constant. Similarly, Fig 14 d) shows that for the HP state equation, the heat flux in the coil C (see fig 1) remains in chaotic regime with small amplitudes for all temperatures, which is due to the effect of the nonlinear function given by Eq (15). It must be emphasized that the previous results apply for the different gases and state equations.

Figure 14

5. Discussion, extension to polar gases and stability

In this section we shall analyze the previously obtained results, their extension to polar gases and the stability.

5.1 Analysis of the results

In section 3, the chaotic behavior has been investigated assuming that the first Lyapunov value is harmonically varied as per Eq (38) and assuming that the equilibrium points P_1 and P_3 are weak focuses (see Fig 2 a)). Now we aim to elucidate whether the device shown in Fig 1 can be used to estimate the virial coefficients and analyze different state equations from another chaotic behaviors obtained through different procedures. To investigate this issue, Eq (7) is modified as follows:

$$\frac{S}{m}\left[F'(t)+F_s\right]=\frac{S^2}{m}\left[P'(t)+P_s\right]-\frac{K}{S^2}\left[V'(t)+V_{se}\right]^2+\frac{S^2}{m}P_{1s} - f_p\frac{b}{m}\frac{dV'(t)}{dt}+A_F\sin\omega_F t \tag{62}$$

where $A_F \sin \omega_F t$ is an external harmonic disturbance applied to the piston. This issue has been investigated in (Pérez-Molina et al., 2016) but at low pressures (rather than with large pressure excursions), for which only the first and second virial coefficients provide helpful information. It should be remarked that the model equations remain

unaltered with the change indicated in Eq (62), whereas the gas presents chaotic behavior for the values $A_F = 0.02$, $\omega_f = 5.2\ rad/s$ and assuming that $f_p = 0$ so that the friction it is not compensated by the control law (62).

Fig 15 shows the simulation results obtained through the PRt state equation. As shown in Fig 15 a), a great pressure excursion for the values of T_s = 300 K and P_s = 100 atm is obtained, whereas the temperature remains approximately constant as shown in Fig 15 b). Nevertheless, it is apparent that the chaotic pressure oscillations are different than the ones shown in Figs 4 a), 4 c), 7 and 11 a). The strange attractor in the phase plane $x_p(t)$-$dx_p(t)/dt$ is plotted in Fig 15 c), and once again it is evident that the chaotic behavior is different to the one of Fig 5 a). Analogous results are obtained for the rest of the considered state equations except for the BB state equation, for which the gas exhibits non-chaotic oscillations for the values $A_F = 0.02$ and $\omega_f = 5.2\ rad/s$.

Figure 15

Table 1 shows an estimation of the first five virial coefficients for the argon, which have been calculated by using all the state equations considered in this work. The first and second virial coefficients are reasonably in accordance with the data of (Dymond et al., 2002; Gosman et al., 1969; Fayazi et al., 2014) for the temperatures $T_s = 300$ and $T_s = 700\ K$ as well as for an initial pressure $P_s = 100\ atm$. In all cases two chaotic behaviors have been assumed, which have been marked as L_y when Eq 7 is used and A_F when Eq (7) is substituted by Eq (62). It is clear that the HP, SRK and RK state equations provide the best results for the first and second virial coefficients compared to the experimental data. On the other hand, the theoretical device of Fig 1 can be used to estimate the virial coefficients regardless the route to chaos used in the calculation of $P(t)$, $T(t)$ and $v(t)$.

Table 1

To corroborate the previous assertions we shall calculate the fugacity coefficient for the methane by using the virial coefficients, and we shall compare it with the fugacity coefficient calculated from the SRK state equation (Dymond et al., 2002;

Soave, 1972; Gosman et al., 1969; Fayazi et al., 2014). For this purpose, the fugacity coefficient *f/P* is defined as:

$$RT\ln\frac{f}{P}=-\int_0^P\left(\frac{RT}{P}-v\right)dP \tag{63}$$

From Eqs (54) and (63) it follows that:

$$\ln\frac{f}{P}=\int_0^P\left(\sum_{i=1}^{n}\frac{C_i(T)}{v^i}\right)\frac{dP}{P} \tag{64}$$

On the other hand, from the virial state equation (54) it is deduced that:

$$\frac{dP}{P}=\frac{RT\left(-\frac{1}{v^2}-\sum_{i=2}^{n}\frac{i\cdot C_i(T)}{v^{i+1}}\right)dv}{RT\left(\frac{1}{v}+\sum_{i=2}^{n}\frac{C_i(T)}{v^i}\right)} \tag{65}$$

Substituting Eq (65) into Eq (64) it is possible to carry out the integration once *dP/P* has been expanded into an arbitrary number of virial terms. Thus considering only the virial coefficients C_1 to C_4, the fugacity coefficient can be approximated as:

$$\ln\frac{f}{P}\approx\frac{C_1}{v}+\frac{C_1^2+C_2}{2v^2}+\frac{3C_1C_2-C_1^3+C_3}{3v^3}+\frac{C_1^4+4C_1C_2-4C_1^2C_2+2C_2^2-C_4}{4v^4} \tag{66}$$

Equation (66) has been used for the methane once the virial coefficients have been calculated from the SRK state equation for *Ts = 300* K and *Ts = 700* K as well as from low to high pressures by using the route to chaos indicated as L_y in table 1. The fugacity coefficients obtained through chaotic behavior have been compared with the ones calculated through the SRK state equation (Soave, 1972, 1984; Span, 2000), which are shown in fig 16 as black points. In addition, several reduced temperatures below the critical temperature and the saturation curve have been plotted with the purpose of contextualizing the simulation data. It can be observed that the coincidence between the

simulations obtained through Eq (66) and the ones calculated with the SRK state equation at $T = 300\ K$ is slightly worse than at $T = 700\ K$. Indeed, this result is in accordance with the fact that the pressure error given by Eq (61) decreases as the temperature increases.

Figure 16

It is interesting to remark that the thermal-physical properties of fluids (specific heat and density) may exhibit great variations near the critical point. However, for all the cases analyzed in the paper the virial coefficients are estimated in a zone far above the critical point, and thus the thermal-physical properties are not affected by trans-critical phenomena. This can be appreciated in Fig 16, where the calculation of the fugacity based on the estimation of the virial coefficients is far away the saturation curve.

5.2 Extension to polar gases

To demonstrate that our methodology also works properly for polar gases, we shall analyze the acetone and the ammonia. For this purpose, we shall use the High Precision (HP) state equation for polar gases given by:

$$P(T,\rho) = -\left(\frac{\partial a(T,\rho)}{\partial v}\right)_T$$

$$FP = P(T,\rho) - \rho RT\left[1 + \delta\left(\frac{\partial \alpha^R(\tau,\delta)}{\partial \delta}\right)_\tau\right] = 0 \ ; \quad \delta = \frac{\rho}{\rho_c} \quad ; \quad \tau = \frac{T_c}{T}$$

$$\alpha^R(\tau,\delta) = n_1\delta\tau^{0.25} + n_2\delta\tau^{1.25} + n_3\delta\tau^{1.5} + n_4\delta^3\tau^{0.25} + n_5\delta^7\tau^{0.875} + \tag{67}$$

$$n_6\delta\tau^{2.375}\exp(-\delta) + n_7\delta^2\tau^2\exp(-\delta) + n_8\delta^5\tau^{2.125}\exp(-\delta) + n_9\delta\tau^{3.5}\exp(-\delta^2)$$

$$+ n_{10}\delta\tau^{6.5}\exp(-\delta^2) + n_{11}\delta^4\tau^{4.75}\exp(-\delta^2) + n_{12}\delta^2\tau^{12.5}\exp(-\delta^3)$$

as well as the Soave (SOA) state equation given in Eq (A6) of the appendix. Figure 17 shows the results obtained for the acetone following the same steps of section 4 with 10 temperatures between 550 K and 750 K as well as an initial pressure of 30 atm to obtain chaotic behavior with the same parameter values of section 3. The results marked with SOA_1 and HP_1 have been respectively obtained through equations (A6) and (67)

assuming that six virial coefficients have been estimated from Eq (56). These results exhibit a similar response to that of Figs 11 a) and b). On the other hand, the pressure for the acetone is calculated through the specific volume and temperatures obtained in the simulation by using the state equations given in Eqs. (A6) and (67), which respectively lead to the virial coefficients SOA_2 and HP_2 by means of Eq (56). As expected, we obtain an exact agreement between SOA_1 and SOA_2 as well as between HP_1 and HP_2. It is interesting to remark that our procedure allows to estimate the virial coefficients in a region where experimental data do not exist, and that it can also be applied to strongly polar gases.

Figure 17

Fig 18 shows the simulation results for the ammonia. The virial coefficients have been calculated for the same temperatures as in the previous case of the acetone, but taking a pressure of 130 atm so that the excursion of pressures is now higher. It should be remarked that the state equation of High Precision leads to values that are almost coincident with the experimental values for coefficient B, whereas the state equation of Soave leads to a higher deviation for the coefficient B (Fig 18 a)). In Fig 18 b) the C coefficient shows a higher deviation with respect to the experimental data, which is logical since there is more uncertainty in the experimental data for the C coefficient.

Figs 18 c) and d) respectively show the relative error for the pressure obtained from the Soave and High precision state equations and the virial expansions taking two and five coefficients. It should be noted that a range of pressures (between 130 atm and 400 atm) with a very small error for the High Precision state equation appears when the number of virial coefficients increases. Similar results are obtained for the oxygen but taking six virial coefficients, as shown in Fig 13 d).

Figure 18

In figure 19 the virial coefficients C_3 to C_6 are plotted for the SOA and HP state equations. It should be noted that there is not a good agreement between the results for the SOA and HP state equations due to the high initial pressure (P_s = 130 atm), since the HP state equation is more accurate than the SOA state equation at high pressures.

Figure 19

5.3 Stability analysis

In this section we shall corroborate the stability of the control structure, and in addition we shall discuss the apparent convergence-divergence of the pressures, specific volumes and piston positions that appear in Figs 4 a)-d), 7, 8 a) and 11 a)-b).

The control force on the mobile piston defined in Eq (7) with $f_p = 1$ leads to three equilibrium points for the piston position with respect to the end of the cylinder: P_1 (0.2352 m), P_2 (0.5154 m) and P_3 (0.7612 m). On one hand, the equilibrium point P_2 is always a unstable saddle (see Fig 2) that cannot be reached. On the other hand, the equilibrium points P_1 and P_3 are weak focuses. Consequently, the stability of P_1 and P_3 depends on the signs of their first Lyapunov values: a positive sign for the Lyapunov value implies an instable equilibrium point while a negative one implies a stable equilibrium point.

In order to obtain a chaotic behavior, the C_0 parameter of the mechanical subsystem is varied harmonically with respect to time (see Eq (38)). This implies that the first Lyapunov values of P_1 and P_3 vary harmonically with respect to time in counterphase, i.e. when the first Lyapunov value of P_1 is positive the first Lyapunov value of P_3 is negative and conversely. Consequently, P_1 is stable when P_3 is unstable and conversely, so the behaviors of P_1 and P_3 are periodically alternating between stable/unstable due to the harmonic variation of their first Lyapunov values. This behavior can be appreciated in fig 20, which shows the (scaled) first Lyapunov values $L_{1P1}(t)/8.10^8$ and $L_{1P3}(t)/8.10^8$ corresponding to P_1 and P_3 respectively. In addition, fig 20 shows the piston position $x_p(t)$, which has been obtained with the refrigerant R22 ($CHClF_2$) as a polar gas and the simulation parameters indicated at legends of Figs 1 and 4.

Figure 20

At t = 0 the piston position is at P_3, and since $L_{1P3}(t)/8.10^8 > 0$ the piston cannot stay at this point and remains with increasing oscillations until it eventually jumps to the equilibrium point P_1, which is stable because its first Lyapunov value is negative (blue curve). At approximately $t = t_1$ the first Lyapunov value of P_1 becomes positive whereas the first Lyapunov value of P_3 becomes negative, so the piston cannot stay at P_1 and tends to jump to P_3 (which occurs at $t = t_2$). Since this motion is chaotic, it is impossible to predict the exact time for the occurrence of a jump. For these reasons, there are transients in the pressure and specific gas volume that sometimes seem to diverge and sometimes seem to converge.

6. Conclusions

In this paper we have presented a mechanical-thermal device from which it is possible to investigate the accurateness of a state equation for non polar real gases through the virial expansion at high pressures. The mechanical subsystem is formed by a cylinder with a mobile piston anchored with a nonlinear spring and a viscous damper, which is actuated by an external nonlinear control force with the purpose of decoupling the mechanical and thermal subsystems. The thermal subsystem is formed by two heating coils, a linear PI controller and another nonlinear control law with the purpose of stabilizing the gas temperature at a prescribed set point.

It has been demonstrated that there are three equilibrium points for the piston position, among which two are weak focuses whereas the third one is always an unstable saddle. This configuration has been used for determining the first Lyapunov value in the mechanical subsystem. By varying harmonically the sign of the first Lyapunov value we have obtained chaotic behavior with large pressure excursions and with an almost constant gas temperature due to the thermal control law.

The chaotic behavior has been corroborated through the sensitive dependence, Lyapunov exponents and the spectral power density by using cubic (RK, SRK, PR, PRt, VDWt) and non-cubic (BB, HP) state equations. To corroborate the correctness of the calculations, it has been checked that the sum of Lyapunov exponents is almost coincident with the mean value of the divergence of the vector field associated to the system. Under the same simulation conditions and parameters, all the state equations

lead to chaotic behavior except the BB equation, for which the simulation parameters must be changed to obtain chaotic oscillations. The almost constant chaotic temperatures are within a narrow range which been used to adjust a desired number of virial coefficients through the least square polynomial.

From the procedure shown in this paper, it has also been corroborated that when only the first and second virial coefficients are adjusted, their values are in very good agreement with the experimental data (specially the first coefficient) for all the investigated state equations except for the BB state equation. These results indicate that the accuracy and reliability of the obtained results depend on the precision of the state equation used for each gas in a certain range of pressures and temperatures. However, when three or more virial coefficients are simultaneously adjusted, the accurateness with respect to experimental data decreases only in the second coefficient.

The estimation of virial coefficients from different state equations shows that with only two virial coefficients at low temperatures (above the critical one) and high pressures, the relative pressure error for any state equation (except for BB) is very high. However, as the number of virial coefficients increases, the error decreases and becomes acceptable for practical purposes. At high temperatures and pressures, the number of virial coefficients can be decreased to obtain a reasonable precision in the gas pressure in comparison with the values directly obtained from the state equation.

Finally, we have presented a brief discussion comparing another method to obtain chaotic behavior and how to use it to estimate the virial coefficients, as well as an extension to polar gases and a stability analysis. It has been concluded that the device analyzed in this work can be used with different chaotic behaviors to analyze different state equations. In addition, we have obtained an easy procedure to verify the accurateness of a state equation expressed in terms of virial coefficients for real gases at high pressures. As an example, the fugacity coefficient for the methane has been calculated with five virial coefficients from the SRK state equation, showing consistent results in accordance with the methodology discussed in the manuscript.

As a concluding remark, the main advantages of our methodology can be summarized as follows: (i) it can be applied to estimate an arbitrary number of virial

coefficients (beyond the coefficients B and C known experimentally), (ii) it allows to obtain the virial expansion even at high pressures through induced chaotic oscillations and (iii) it allows to elucidate a pressure range for the applicability of a particular state equation.

Appendix

In this appendix we shall define the parameters of the cubic equations given by Eq (44). In all equations, $T_r = T/T_c$ and $P_r = P/P_c$ respectively denote the reduced temperature and reduced pressure, whereas T_c and P_c are the critical temperature and critical pressure respectively.

i) State equation of Redlich-Kwong (RK)

$$\Theta(T) = a\alpha(T_r)\ ;\ \delta_1 = b\ :\ \varepsilon = 0\ ;\ a = 0.42748\frac{(RT_c)^2}{P_c}\ ;\ b = 0.08664\frac{RT_c}{P_c}$$
$$\alpha(T_r) = \frac{a}{T_r^{0.5}} \qquad \text{(A1)}$$

ii) State equation Soave-Redlich-Kwong (SRK)

$$\Theta(T) = a\alpha(T_r)\ ;\ \delta_1 = b\ :\ \varepsilon = 0\ ;\ a = 0.42748\frac{(RT_c)^2}{P_c}\ ;\ b = 0.08664\frac{RT_c}{P_c}$$
$$\alpha(T_r) = \left[1+\left(0.48+1.574\omega-0.176\omega^2\right)\left(1-T_r^{0.5}\right)\right]^2 \qquad \text{(A2)}$$

iii) State equation Peng-Robinson (PR)

$$\Theta(T) = a\alpha(T_r)\ ;\ \delta_1 = 2b\ :\ \varepsilon = -b^2\ ;\ a = 0.45724\frac{(RT_c)^2}{P_c}\ ;\ b = 0.0778\frac{RT_c}{P_c}$$
$$\alpha(T_r) = \left[1+\left(0.37464+1.5423\omega-0.2669\omega^2\right)\left(1-T_r^{0.5}\right)\right]^2 \qquad \text{(A3)}$$

iv) State equation Peng-Robinson with translation volume (PRt)

$$\Theta = a\alpha\left(T_r\right)\ ;\ a = 0.45724\frac{\left(RT_c\right)^2}{P_c}\ ;\ b\ =\ 0.0778\frac{RT_c}{P_c}$$

$$m_i\ =\ 0.384401\ +\ 1.522760\omega\ -\ 0.213808\omega^2\ +\ 0.034616\omega^3\ -\ 0.001976\omega^4$$

$$\alpha\left(T_r\right) = a\left[1-m_i\left(1-T_r\right)^{0.5}\right]^2$$

$$t_0 = \frac{RT_c}{P_c}(\text{-}0.014471\ +\ 0.067498\omega\ -\ 0.084852\omega^2\ +\ 0.067298\omega^3\ -\ 0.017366\omega^4)$$

$$t_1 = \frac{RT_c}{P_c}\left[\left(\frac{3}{8}\right)-z_c\right]\ ;\ \beta = -10.244700-28.631200\omega\ ;\ t = t_0 + (t_1-t_0)\exp(\beta\left|1-T_c\right|);$$

$$\delta_1 = 2\left(t+b\right)\ ;\ \varepsilon\ =\ V_t^2$$

(A4)

where V_t is the translated volume, z_c is the critical compressibility coefficient and ω is the acentric factor.

v) State equation of Van der Waals with translation volume (VDWt)

$$\Theta = a\alpha\left(T_r\right)\ ;\ a = \frac{27}{64}\frac{\left(RT_c\right)^2}{P_c}\ ;\ b\ =\ \frac{1}{8}\frac{RT_c}{P_c}\ ;\ m_i\ =\ 0.48533\ +\ 1.62400\omega\ -\ 0.21884\omega^2$$

$$\alpha\left(T_r\right) = a\left[1-m_i\left(1-T_r\right)^{0.5}\right]^2\ ;\ t_0 = \frac{RT_c}{P_c}(0.0348+0.0937\omega-0.1661\omega^2+0.1250\omega^3)$$

$$t_1 = \frac{RT_c}{P_c}\left[\left(\frac{3}{8}\right)-z_c\right]\ ;\ z_c = 0.2890-0.0701\omega-0.0207\omega^2\ ;\ \beta = 10.244700\ -28.631200\omega\ ;$$

$$t = t_0 + (t_1-t_0)\exp(\beta\left|1-T_c\right|)\ ;\ \delta_1 = 2\left(t+b\right)\ ;\ \varepsilon\ =\ V_t^2$$

(A5)

vi) State equation of Soave (SOA)

$$\Theta\left(T\right) = a\alpha\left(T_r\right)\ ;\ \delta_1 = b\ ;\ a = 0.42118\frac{\left(RT_c\right)^2}{P_c}$$

$$b = 0.08333\frac{RT_c}{P_c}\ \ ;\ \ \varepsilon = 0.001736\left(\frac{RT_c}{P_c}\right)^2 \qquad \text{(A6)}$$

$$\alpha\left(T_r\right) = \left[1+\left(0.4998+1.5928\omega-0.19563\omega^2+0.025\omega^3\right)\left(1-T_r^{0.5}\right)\right]^2$$

References

Abbot, M., M., 1979. Cubic Equation of State: An Interpretive Review. Equations of State in Engineering and Research. Adv. In Chem. Ser. 182 K. C. Chao, R. L. Robinson eds. American Chemical Society, Washington.

Albertos P., Sala, A., 2004.Multivariable Control Systems, Springer, London.

Annamalai, K., Puri, I., K., 2002. Advanced Thermodynamics Engineering, second ed. CRC Press, Boca Raton, Florida.

Beattie, J., A., Bridgeman, O., C., 1927. A new equation of state for solids, Am. Chem. Soc. J. 49, 1665-1667.

Belanger P., W., Singley C., D., Misovich M., J., 1994. Coexistence curve predicted by the soave-Redlich-Kwong equation in the critical limit, Chem. Eng. Science, 49, 3787-3789.

Benettin G., Galgani L., Giorgilly A., Strelcyn J., M., 1980. Lyapunov characteristic exponents for smooth dynamical systems and for Hamiltonian systems: a method for computing all of them, part I: theory, Meccanica 15, 9–20.

Benettin G., Galgani L., Giorgilly A., Strelcyn J., M., 1980. Lyapunov characteristic exponents for smooth dynamical systems and for Hamiltonian systems: a method for computing all of them, part II: numerical applications, Meccanica 15, 21–30.

Chen, L., Zhang X. R., Cao, S. Bai, H., 2012. Study of trans-critical CO_2 natural convective flow with unsteady heat input and its implications on system control, I. J. Heat Mass Transfer, 55, 7119-7132.

Dymond, J., H., Smith, E., B., 1980. The Virial Coefficients of Pure Gases and Mixtures: A Critical Compilation, Clarendon Press.

Dymond, J., H., Marsh, K., N., Wilhoit, R., C., Wong, K., C., 2002. Virial Coefficients of Pure Gases and Mixtures, Springer_Verlag, Berlin.

Elliot J., R., Daubert T., E., 1985. Revised Procedures for Phase Equilibrium Calculations with the Soave Equation of State, Ind. Eng. Chem. Process Des. Dev. 24, 743-753.

Fayazi A., Arabloo M., Mohammadi A., H., 2014. Efficient estimation of natural gas compressibility factor using a rigorous method, Journal of Natural Gas Science and Engineering, 16, 8-17.

Gmehling, J., Kolbe, B., Kleiber, M., Rarey, J., 2012. Chemical Thermodynamics, Wiley-VCH Verlag, Weinheim, Germany.

Goodwin, A., R., H., Sengres, J., V., Peters C., J., ed., 2010. Applied Thermodynamics of Fluids, RSC Publishing, Cambridge.

Gosman A., I., McCarty R., D., Hust J., G., 1969. Thermodynamic Properties of Argon. From the Triple Point to 300 K at Pressures up to 1000 Atmospheres, Cryogenic Division. Institute for Basic Standars NSRDS 1-32.

Guckenheimer, J., Holmes, P., 1983. Nonlinear Oscillations, Dynamical Systems and Bifurcations of Vector Fields, Springer, New York.

Holleran E., 2007. Improved virial coefficients, Fluid Phase Equilibria, 251 29–32.

Hougen O., A., Watson, K., M., Ragatz, R., A., 1954. Industrial Chemical Calculations, Vol. II Thermodynamics, second ed., John Wiley & Sons, New York.

Lichtenberg A., J., Lieberman M.. A., 1992. Regular and chaotic dynamics, second ed., Springer-Verlag, New York.

Mason, E., A., Spurling, T., H., 1968. The Virial Equation of State, Pergamon, New York.

Meng L., Duan Y-Y., Li L., 2004. Correlations for second and third virial coefficients of pure fluids, Fluid Phase Equilibria 226, 109–120.

Peng D-Y., Robinson, D., B., 1976. A New Two-Constant Equation of State, Ind. Eng. Chem., Fundam. 15, 59-64.

Pérez-Polo M., F., Albertos P., 2007, Nonisothermal Stirred- Tank Reactor with Irreversible Exothermic Reaction A → B: Nonlinear Phenomena in: H. O. Méndez-Acosta, R. Femat, V. Gónzalez –Álvarez (Eds), Lecture Notes in Control and Information Sciences, nº 361, Springer-Verlag, Berlin, Heilderberg, pp. 276-279.

Pérez-Molina, M., Gil-Chica J., Fernández-Varó, E., Pérez-Polo M., F., 2016. Steady state, oscillations and chaotic behavior of a gas inside a cylinder with a mobile piston controlled by PI and nonlinear control, Commun. Nonlinear Sci. Numer. Simulat. 36, 468–495.

Pérez-Polo M., F., Pérez-Molina M., 2014. Steady-state self oscillations and chaotic behavior of a controlled electromechanical device by using the first Lyapunov value and the Melnikov theory, Journal of Sound and Vibration, 333, 1163-1181.

Poling, B., E., Prausnitz, J., M., Connell, J., P., O., 2001.The Properties of Gases and Liquids, fifth ed. Mc-Graw Hill, New York.

Prausnitz, J., M., Lichtenthaler, R., N., Gomes de Azevedo E., 2000. Molecular Thermodynamics of Fluid-Phse Equilibria, third ed., Prentice Hall, New York.

Redlich, O., Kwong, J., N., S., 1948. On the Thermodinamics of Solutions. V: An Equation of State. Fugacities of Gaseous Solutions, Symposium on Thermodynamics and Molecular Structure of Solutions, 114th Meeting of the American Chemical Society, Portland, Oregon, September 13 and 14.

Soave, G., 1972. Equilibrium constants from a modified Redlich-Kwong equation of state, Chem. Eng. Science 27, 1197-1203.

Soave, G., 1984. Improvement of the Van Der Waals equation of state, Chem. Eng. Science 39, 357-369.

Span, R., 2000. Multiparameter Equations of State. An Accurate Source of Thermodynamic Property Data, Springer-Verlag.

Su, G-J., Chang C-H., 1946. Generaized Beattie-Bridgeman Equation of State for Real Gases, J. Am. Chem. Soc. 68, 1080-1083.

Tassios, D., 1993. Applied Chemical Engineering Thermodynamics, Springer-Verlag, Berlin,.

Tsonopoulos, C., Heidman, J., L., 1985. From Redlich-Kwong to the Present, Fluid Phase Equilib. 24, 1-15.

Valderrama J., O., 1990. A Generalized Patel-Teja Equation of State for Polar and Nonpolar Fluids and Mixtures, J. Chem. Eng. Japan, 23, 87-91.

Valderrama, J., O., 2003. The State of the Cubic Equations of State, Ind. Eng. Chem. Res. 42, 1603-1618.

Wei, Y., S., Sadus, R., J., 2000. Equations of State for the Calculation of Fluid-Phase Equilibria, AIChE Journal 46, 160-196.

Wiggins S., 2000. Introduction to Applied Nonlinear Dynamical Systems and Chaos, second ed.. Springer, New York.

Yaws C., L., 1999. Chemical Properties Handbook, McGraw-Hill, New York.

Table 1
Virial coefficients C_i (liter/mole) for different state equations
***Data obtained from experimental values**
L_y Chaotic behavior with the first Lyapunov value
A_F Chaotic behavior with harmonic disturbance

	T_s = 300 K	$C_1.10^2$	$C_2.10^3$	$C_3.10^5$	$C_4.10^6$	$C_5.10^8$
	Ar	**-1.5200***	**1.080***			
RK	L_y	-1.5965	1.0154	3.9205	-2.3442	6.7358
100 atm	A_F	-1.5795	0.9264	5.2228	-2.9932	7.7493
SRK	L_y	-1.2383	0.9029	4.3994	-2.4533	6.7848
100 atm	A_F	-1.2413	0.8920	4.8414	-2.7441	7.3110
PR	L_y	-1.8673	1.6232	0.8407	-1.7286	6.2605
100 atm	A_F	-1.8593	1.5727	1.6915	-2.1871	7.0027
PRt	L_y	-2.5937	6.4733	-0.3033	7.2405	-3.5305
100 atm	A_F	-2.4413	6.3082	-0.2576	4.5672	2.4046
VDWt	L_y	-3.5020	1.8578	-5.4036	0.7642	-0.4192
100 atm	A_F	-1.0563	0.6267	8.0107	-4.2456	0.1052
BB	L_y**	-1.5434	1.1880	-0.7198	0.3326	-0.4627
100 atm	A_F**	-0.8635	-1.5086	0.3155	-0.1615	0.3017
HP	L_y	-1.5642	1.4658	7.7976	-1.8525	5.4314
100 atm	A_F	-1.5709	1.4917	7.5036	-1.7247	5.2474
	T_s = 700 K	$C_1.10^2$	$C_2.10^3$	$C_3.10^5$	$C_4.10^6$	$C_5.10^8$
	Ar	**1.5100***	**0.6044***			
RK	L_y	1.1089	0.7116	0.6644	0.2031	1.0544
100 atm	A_F	1.1071	0.7222	0.4867	0.3236	0.7452
SRK	L_y	1.7264	0.5777	0.9216	0.1836	0.9843
100 atm	A_F	1.7248	0.5879	0.7475	0.2993	0.7106
PR	L_y	1.3875	0.7884	-0.2713	0.6150	0.2039
100 atm	A_F	1.3954	0.7991	-0.4101	0.6638	0.2237
PRt	L_y	1.5452	0.9536	0.1093	-0.1226	0.4307
100 atm	A_F	1.5416	0.9806	0.1022	-0.1152	0.4103
VDWt	L_y	1.8355	0.5942	1.1898	0.1642	1.3348
100 atm	A_F	1.8338	0.6023	1.0920	0.1771	1.4705
BB**	L_y**	1.6741	0.4290	3.2677	-5.1652	0.2975
100 atm	A_F**	1.6887	0.3013	6.9775	-9.4213	0.4599
HP	L_y	1.5398	0.7716	5.9163	-0.2220	0.5041
100 atm	A_F	1.5382	0.7785	5.8762	-0.2761	0.8987

** Values obtained from non-chaotic oscillations

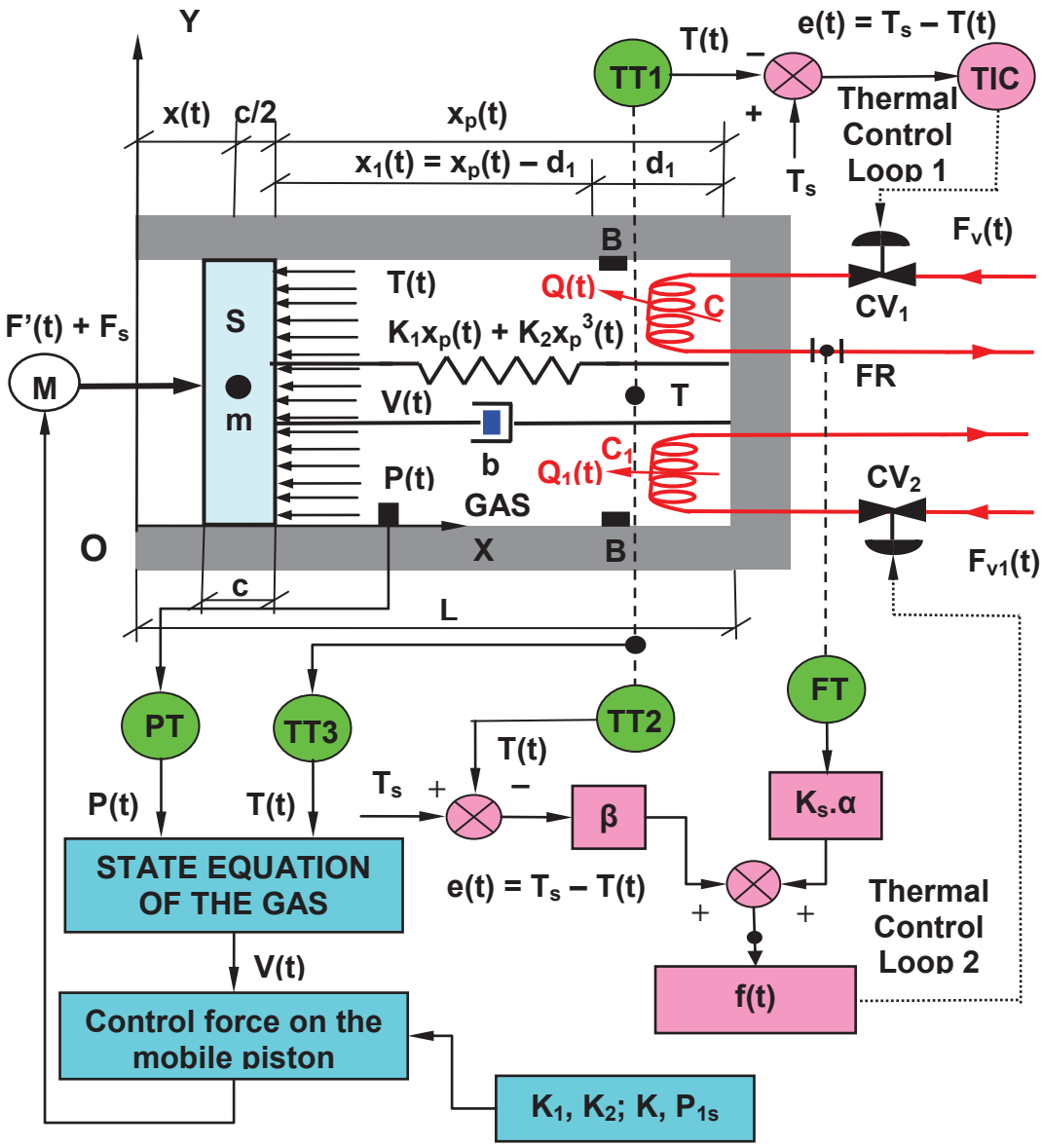
Y
x(t)
c/2
$x_p(t)$
$x_1(t) = x_p(t) - d_1$
d_1
B
T(t)
Q(t)
C
$K_1x_p(t) + K_2x_p^3(t)$
V(t)
T
b
C_1
$Q_1(t)$
P(t)
GAS
X
B
O
c
L
S
m
M
F'(t) + F_s
TT1
T(t)
e(t) = T_s – T(t)
TIC
Thermal Control Loop 1
T_s
$F_v(t)$
CV_1
FR
CV_2
$F_{v1}(t)$
PT
TT3
TT2
FT
P(t)
T(t)
T_s
T(t)
β
$K_s.\alpha$
e(t) = T_s – T(t)
Thermal Control Loop 2
STATE EQUATION OF THE GAS
V(t)
f(t)
Control force on the mobile piston
K_1, K_2; K, P_{1s}

Figure 1

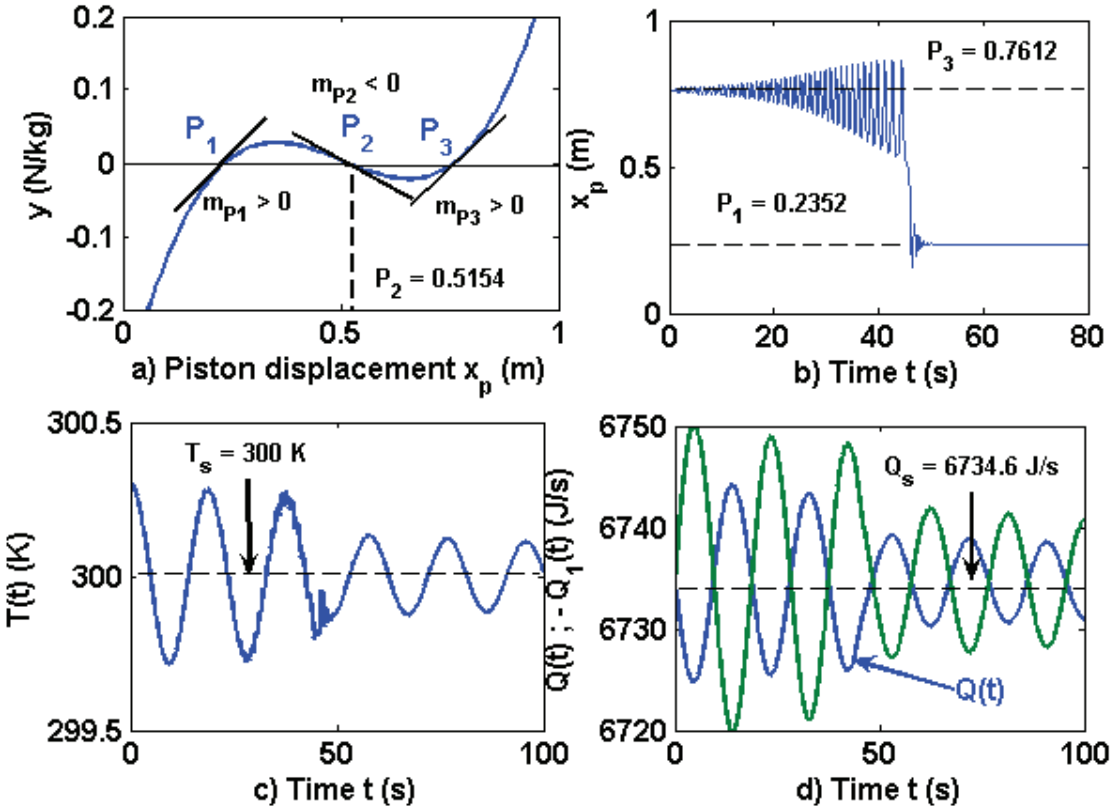
0.2
0.1
0
-0.1
-0.2
y (N/kg)
P1
P2
P3
mP2 < 0
mP1 > 0
mP3 > 0
P2 = 0.5154
0
0.5
1
a) Piston displacement xp (m)
1
0.5
0
xp (m)
P3 = 0.7612
P1 = 0.2352
0
20
40
60
80
b) Time t (s)
300.5
300
299.5
T(t) (K)
Ts = 300 K
0
50
100
c) Time t (s)
6750
6740
6730
6720
Q(t) ; - Q1(t) (J/s)
Qs = 6734.6 J/s
Q(t)
0
50
100
d) Time t (s)

Figure 2

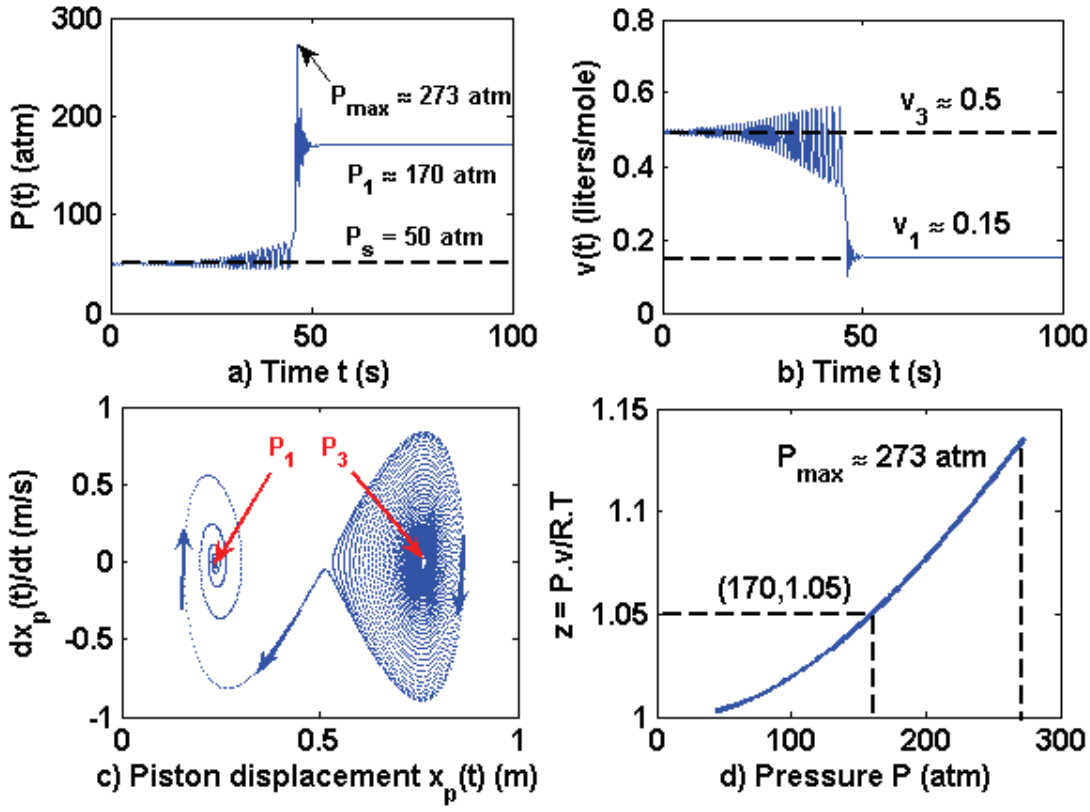
P(t) (atm)
$P_{max} \approx 273$ atm
$P_1 \approx 170$ atm
$P_s = 50$ atm
a) Time t (s)
v(t) (liters/mole)
$v_3 \approx 0.5$
$v_1 \approx 0.15$
b) Time t (s)
$dx_p(t)/dt$ (m/s)
P_1
P_3
c) Piston displacement $x_p(t)$ (m)
z = P.v/R.T
$P_{max} \approx 273$ atm
(170,1.05)
d) Pressure P (atm)

Figure 3

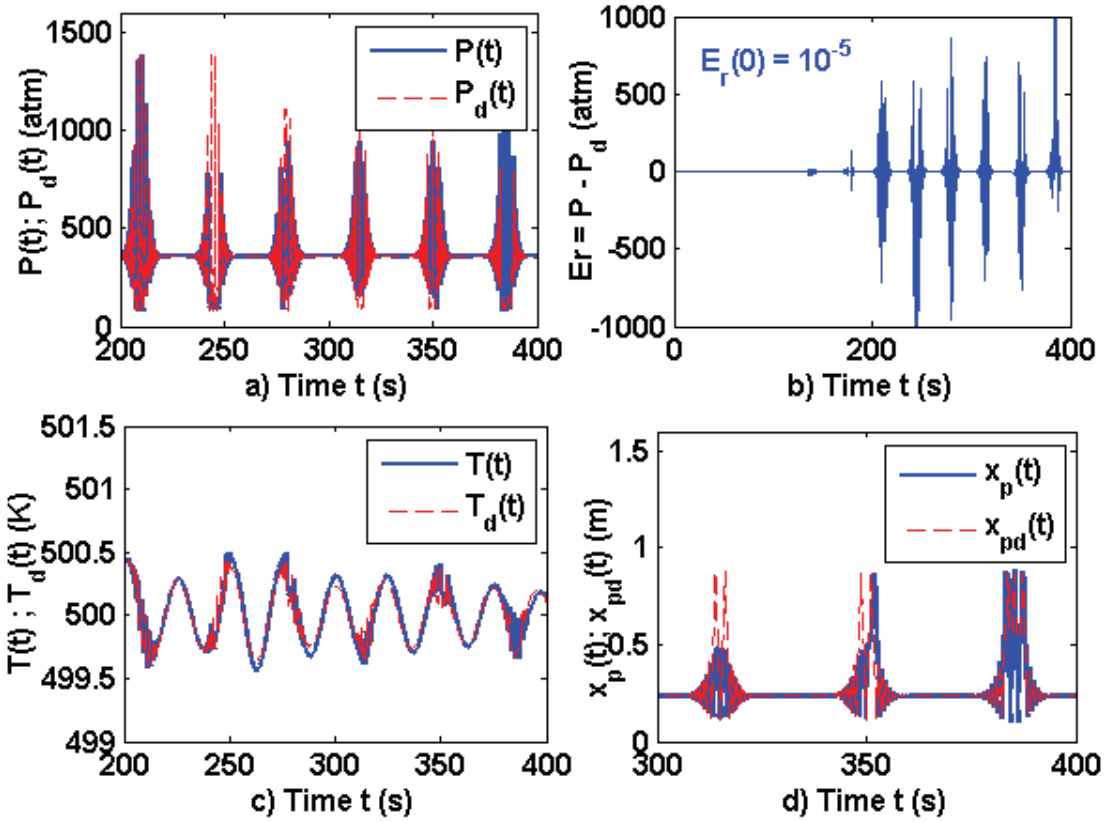
P(t)
P_d(t)
P(t); P_d(t) (atm)
a) Time t (s)
E_r(0) = 10^-5
Er = P - P_d (atm)
b) Time t (s)
T(t)
T_d(t)
T(t) ; T_d(t) (K)
c) Time t (s)
x_p(t)
x_pd(t)
x_p(t); x_pd(t) (m)
d) Time t (s)

Figure 4

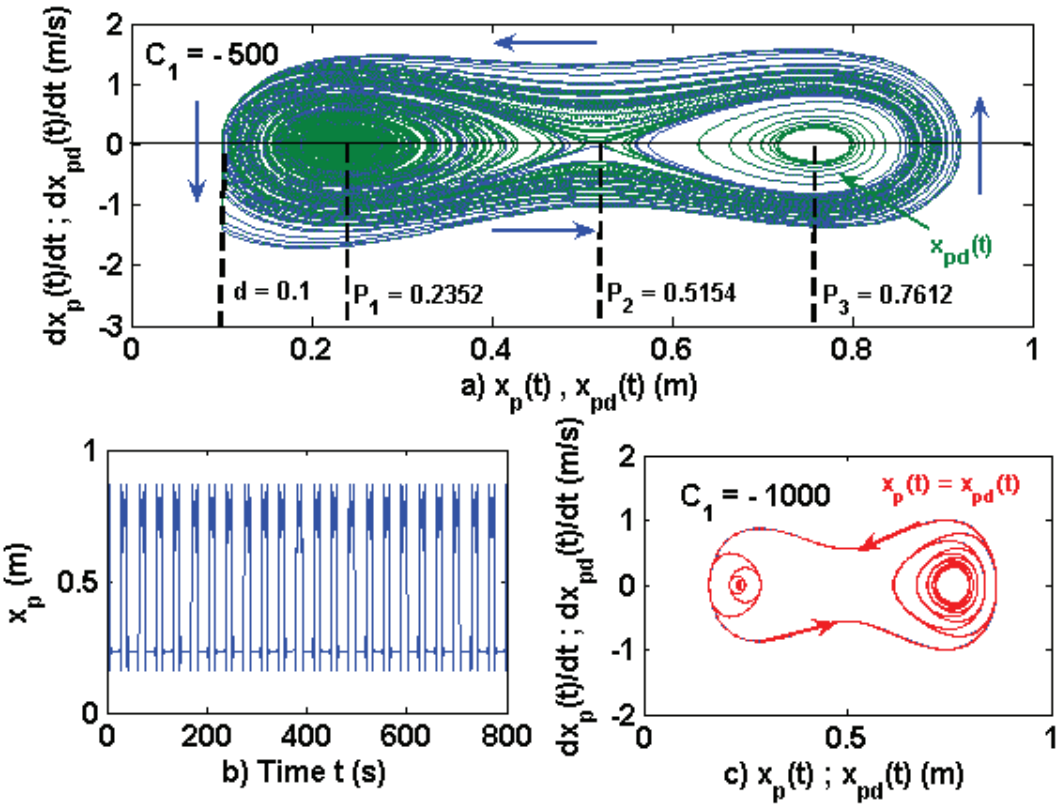
C1 = - 500
d = 0.1
P1 = 0.2352
P2 = 0.5154
P3 = 0.7612
xpd(t)
dxp(t)/dt ; dxpd(t)/dt (m/s)
a) xp(t) , xpd(t) (m)
xp (m)
b) Time t (s)
C1 = - 1000
xp(t) = xpd(t)
dxp(t)/dt ; dxpd(t)/dt (m/s)
c) xp(t) ; xpd(t) (m)

Figure 5

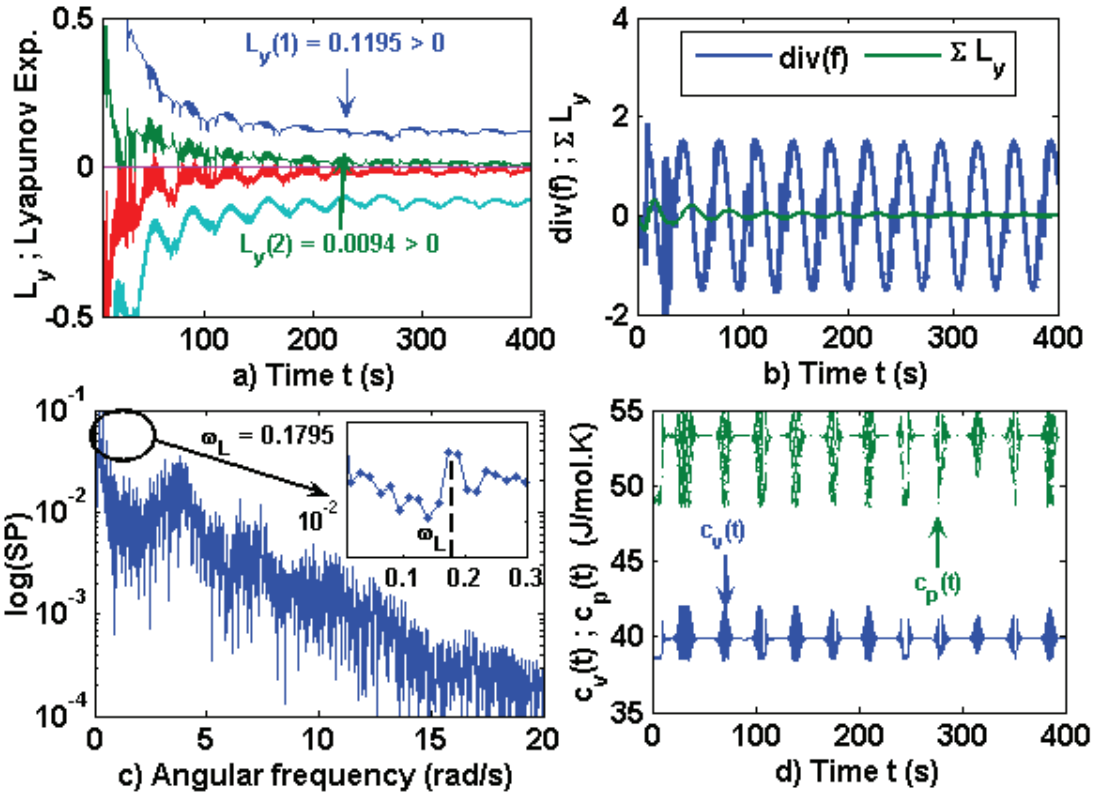
L_y ; Lyapunov Exp.
L_y(1) = 0.1195 > 0
L_y(2) = 0.0094 > 0
a) Time t (s)
div(f) ; Σ L_y
div(f)
Σ L_y
b) Time t (s)
log(SP)
ω_L = 0.1795
10^-2
ω_L
c) Angular frequency (rad/s)
c_v(t) ; c_p(t) (J/mol.K)
c_v(t)
c_p(t)
d) Time t (s)

Figure 6

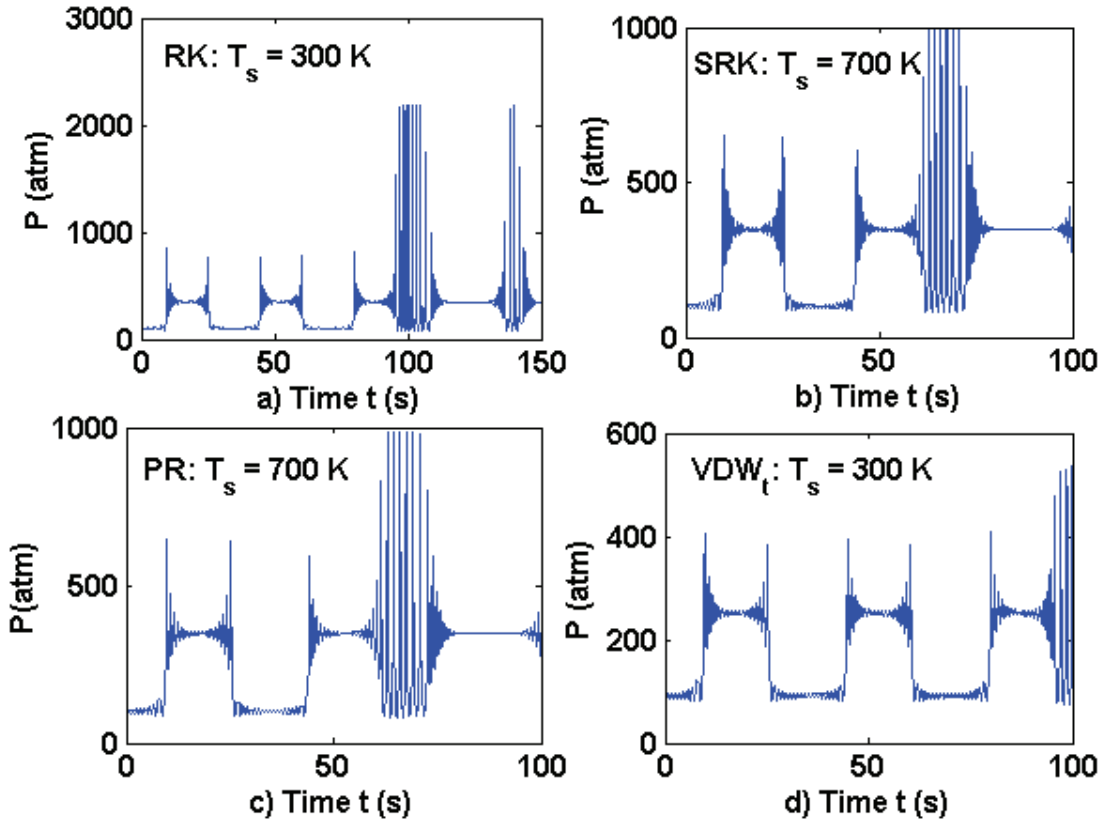
RK: T_s = 300 K
P (atm)
a) Time t (s)
SRK: T_s = 700 K
P (atm)
b) Time t (s)
PR: T_s = 700 K
P(atm)
c) Time t (s)
VDW_t: T_s = 300 K
P (atm)
d) Time t (s)

Figure 7

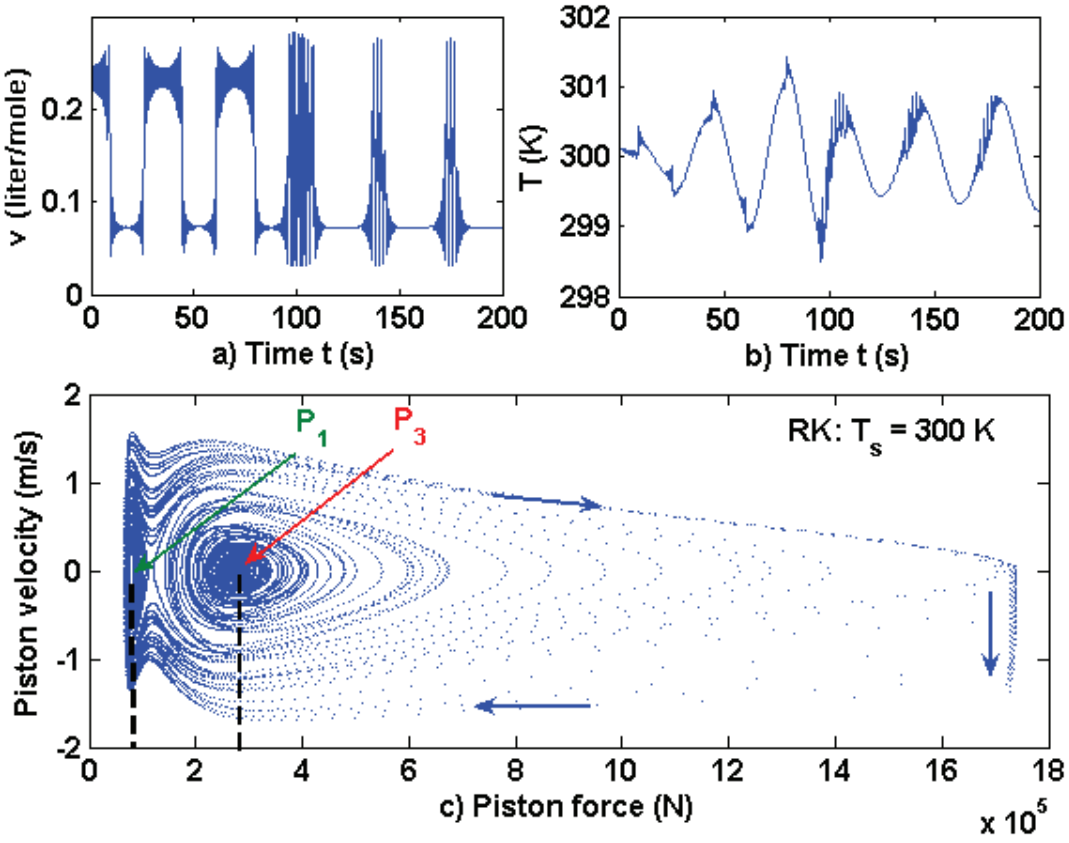
v (liter/mole)
0.2
0.1
0
0
50
100
150
200
a) Time t (s)
T (K)
302
301
300
299
298
0
50
100
150
200
b) Time t (s)
Piston velocity (m/s)
2
1
0
-1
-2
P1
P3
RK: Ts = 300 K
0
2
4
6
8
10
12
14
16
18
c) Piston force (N)
x 10^5

Figure 8

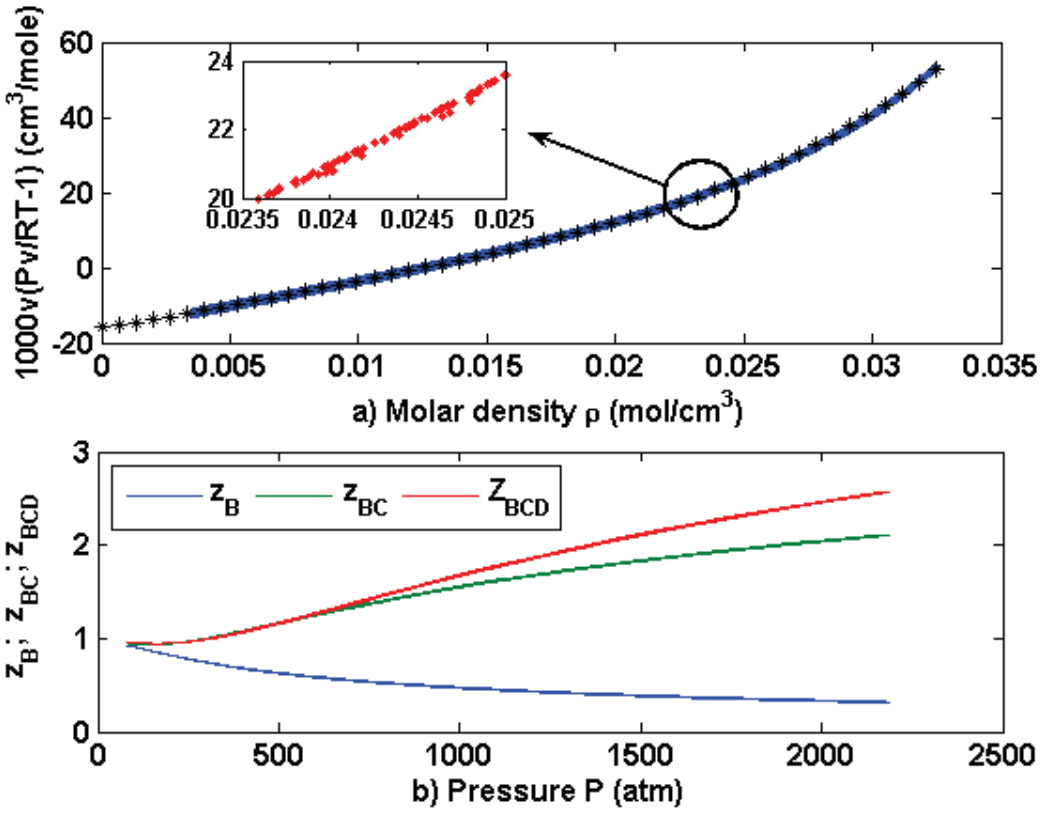
1000v(Pv/RT-1) (cm3/mole)
60
40
20
0
-20
0
0.005
0.01
0.015
0.02
0.025
0.03
0.035
24
22
20
0.0235
0.024
0.0245
0.025
a) Molar density ρ (mol/cm3)
zB; zBC; zBCD
3
2
1
0
zB
zBC
ZBCD
0
500
1000
1500
2000
2500
b) Pressure P (atm)

Figure 9

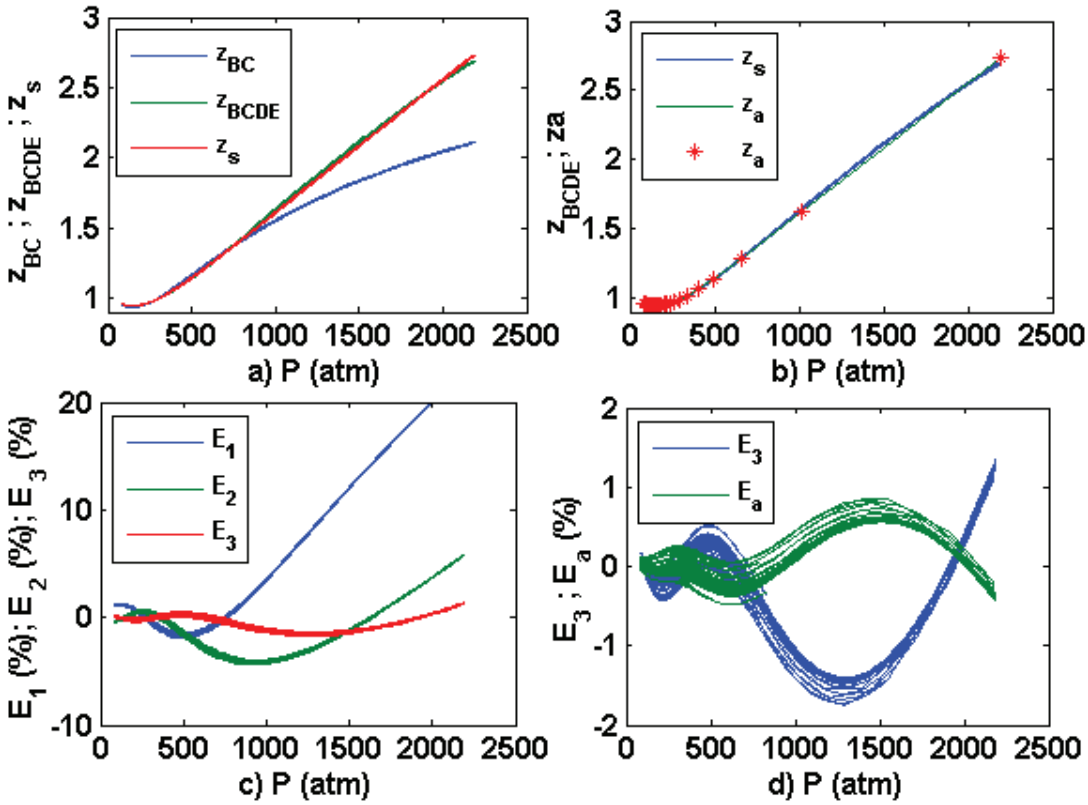
z_BC ; z_BCDE ; z_s
z_BC
z_BCDE
z_s
a) P (atm)
z_BCDE ; za
z_s
z_a
z_a
b) P (atm)
E_1 (%); E_2 (%); E_3 (%)
E_1
E_2
E_3
c) P (atm)
E_3 ; E_a (%)
E_3
E_a
d) P (atm)

Figure 10

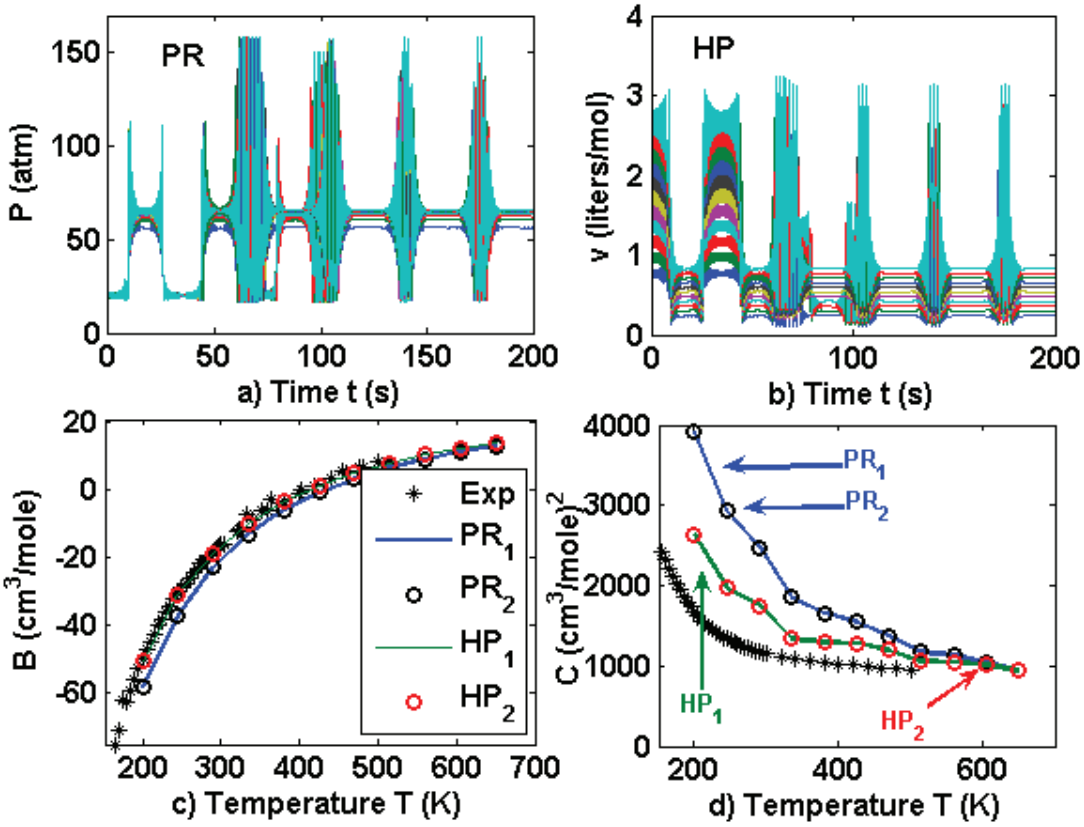
PR
P (atm)
a) Time t (s)
HP
v (liters/mol)
b) Time t (s)
B (cm3/mole)
Exp
PR1
PR2
HP1
HP2
c) Temperature T (K)
C (cm3/mole)2
PR1
PR2
HP1
HP2
d) Temperature T (K)

Figure 11

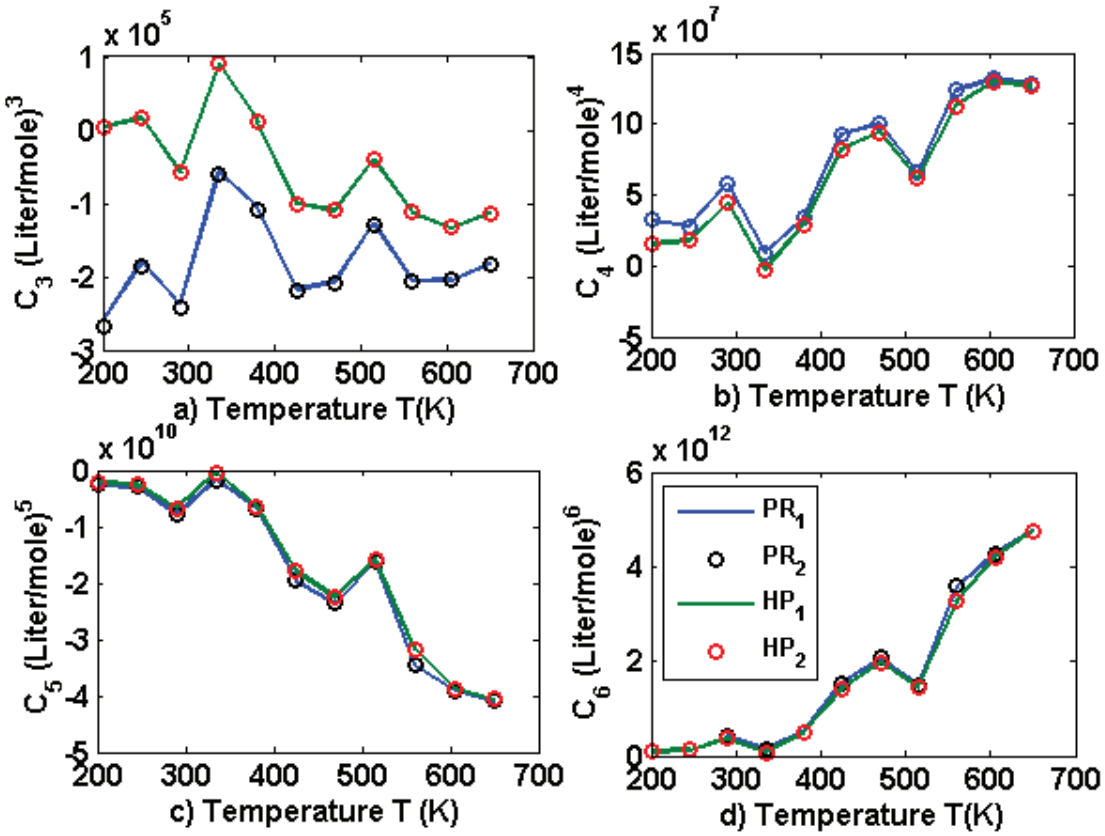
x 10^5
C3 (Liter/mole)^3
a) Temperature T(K)
x 10^7
C4 (Liter/mole)^4
b) Temperature T (K)
x 10^10
C5 (Liter/mole)^5
c) Temperature T (K)
x 10^12
C6 (Liter/mole)^6
d) Temperature T(K)
PR1
PR2
HP1
HP2

Figure 12

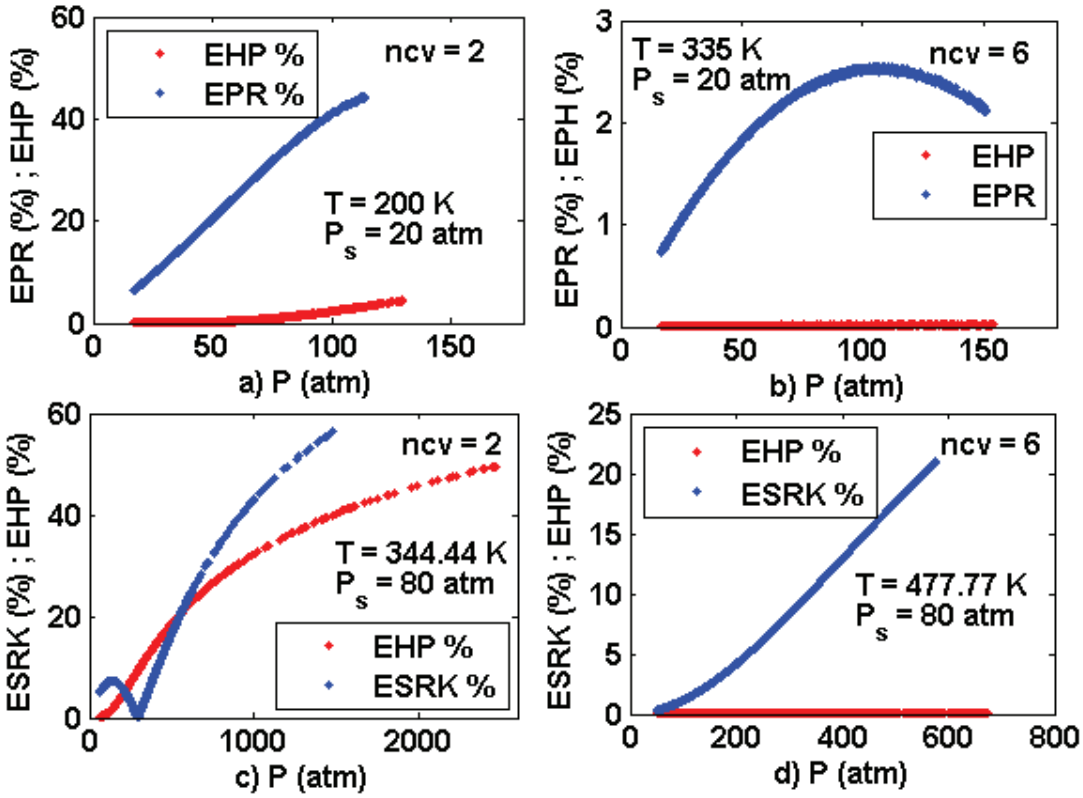
EHP %
EPR %
ncv = 2
T = 200 K
P_s = 20 atm
EPR (%) ; EHP (%)
a) P (atm)
T = 335 K
P_s = 20 atm
ncv = 6
EHP
EPR
EPR (%) ; EPH (%)
b) P (atm)
ncv = 2
T = 344.44 K
P_s = 80 atm
EHP %
ESRK %
ESRK (%) ; EHP (%)
c) P (atm)
EHP %
ESRK %
ncv = 6
T = 477.77 K
P_s = 80 atm
ESRK (%) ; EHP (%)
d) P (atm)

Figure 13

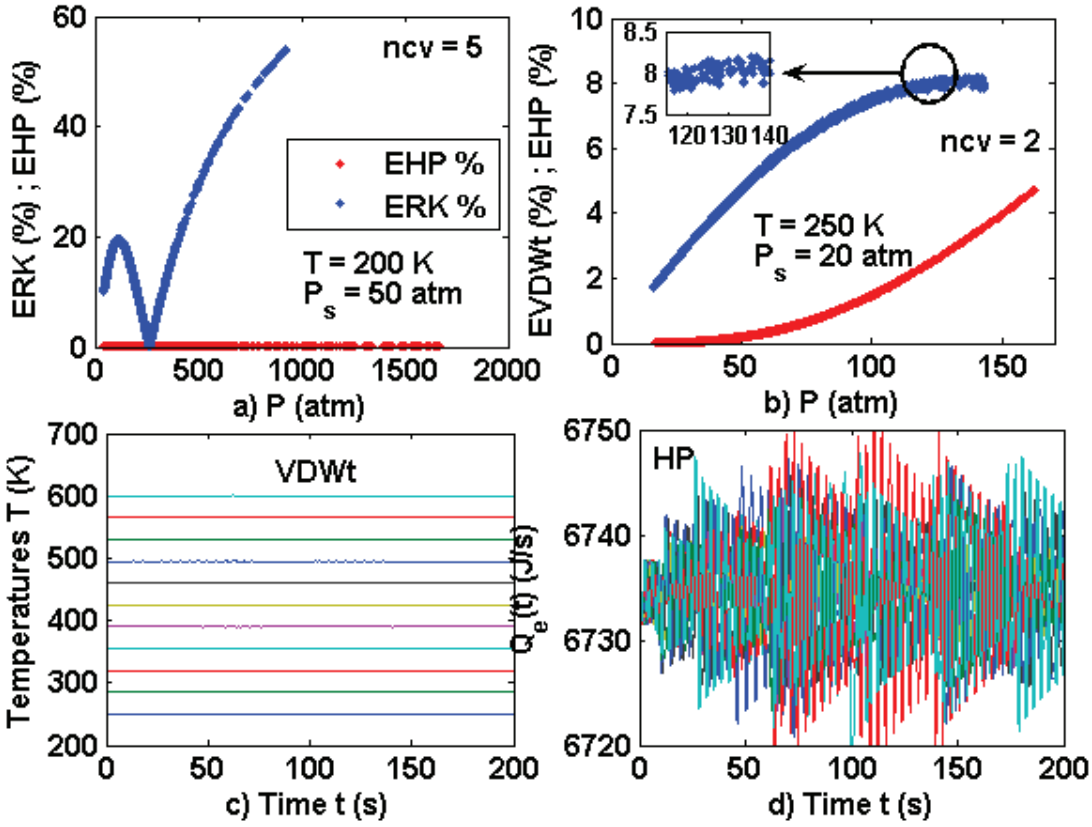
ncv = 5
EHP %
ERK %
T = 200 K
P s = 50 atm
ERK (%) ; EHP (%)
a) P (atm)
ncv = 2
T = 250 K
P s = 20 atm
EVDWt (%) ; EHP (%)
b) P (atm)
VDWt
Temperatures T (K)
c) Time t (s)
HP
Q e (t) (J/s)
d) Time t (s)

Figure 14

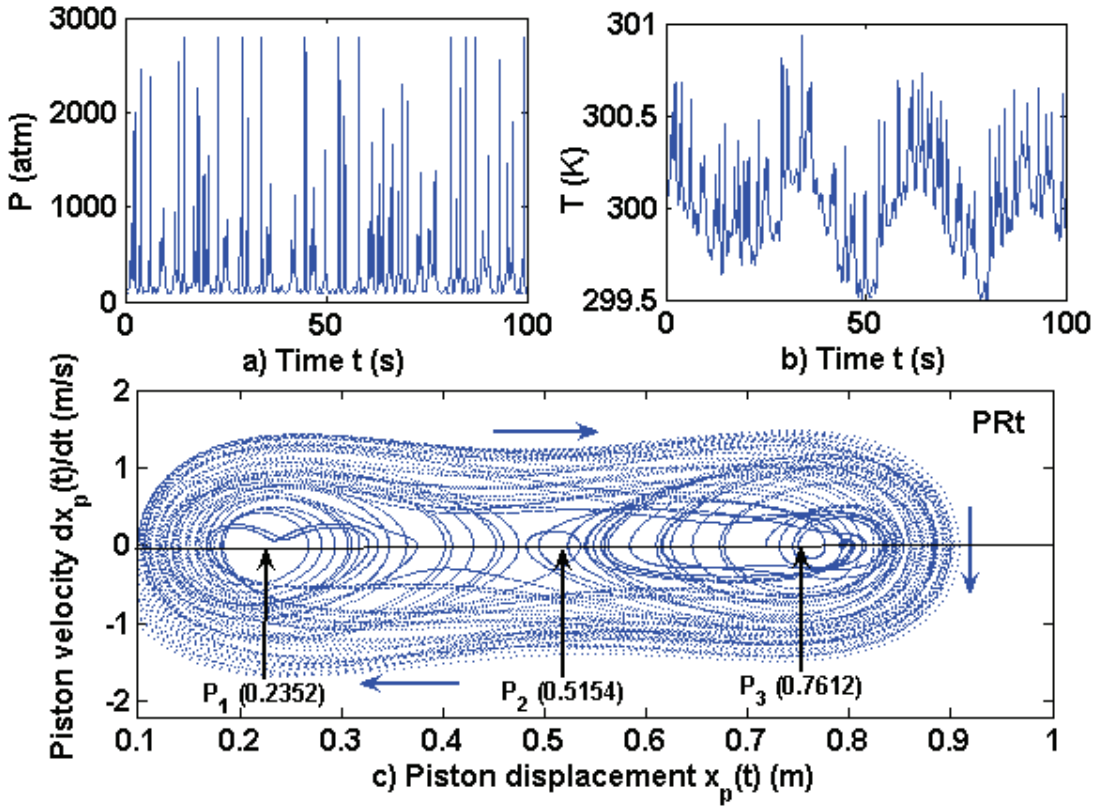
P (atm)
3000
2000
1000
0
0
50
100
a) Time t (s)
T (K)
301
300.5
300
299.5
0
50
100
b) Time t (s)
Piston velocity dx_p(t)/dt (m/s)
2
1
0
-1
-2
PRt
P1 (0.2352)
P2 (0.5154)
P3 (0.7612)
0.1
0.2
0.3
0.4
0.5
0.6
0.7
0.8
0.9
1
c) Piston displacement x_p(t) (m)

Figure 15

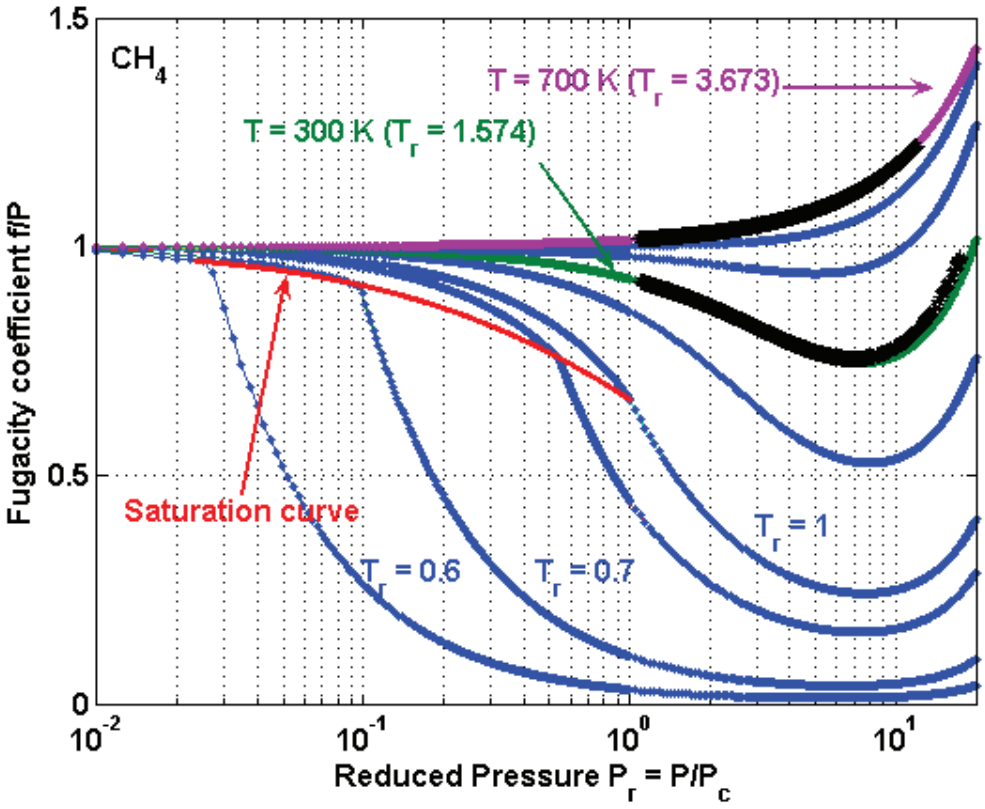
CH4
T = 700 K (Tr = 3.673)
T = 300 K (Tr = 1.574)
Saturation curve
Tr = 1
Tr = 0.6
Tr = 0.7
Fugacity coefficient f/P
Reduced Pressure Pr = P/Pc
1.5
1
0.5
0
10-2
10-1
100
101

Figure 16

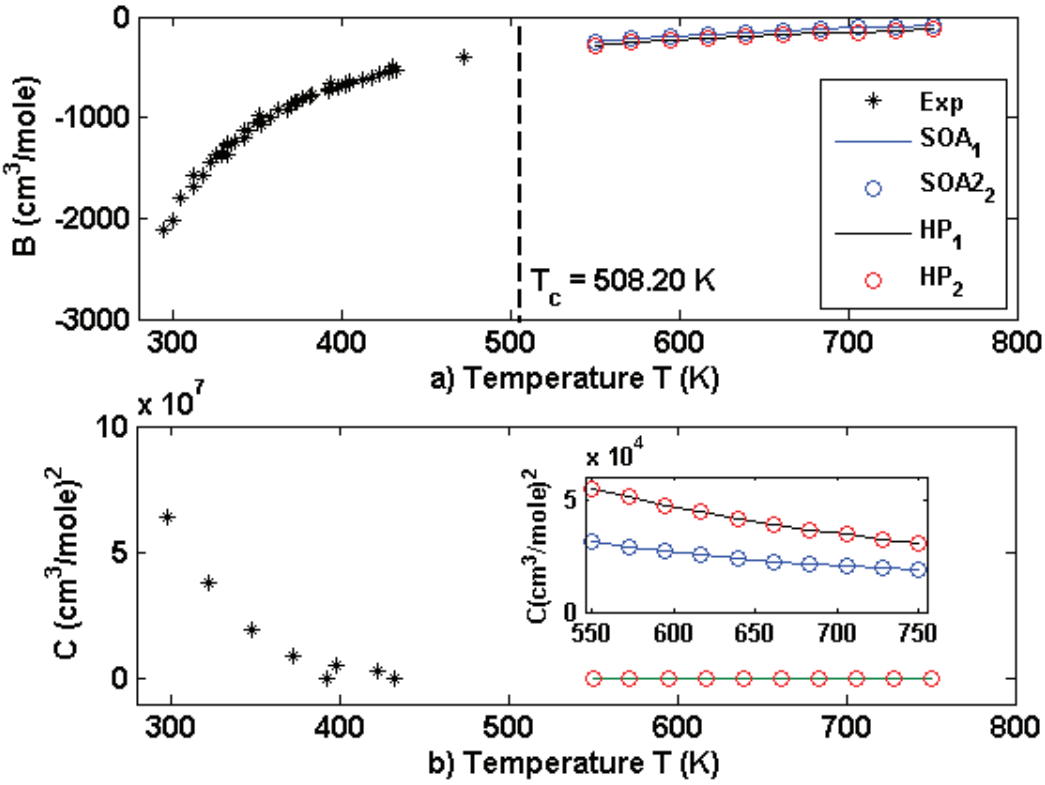
B (cm3/mole)
0
-1000
-2000
-3000
300
400
500
600
700
800
a) Temperature T (K)
Exp
SOA1
SOA22
HP1
HP2
Tc = 508.20 K
x 10^7
C (cm3/mole)2
10
5
0
x 10^4
C(cm3/mole)2
5
0
550
600
650
700
750
b) Temperature T (K)

Figure 17

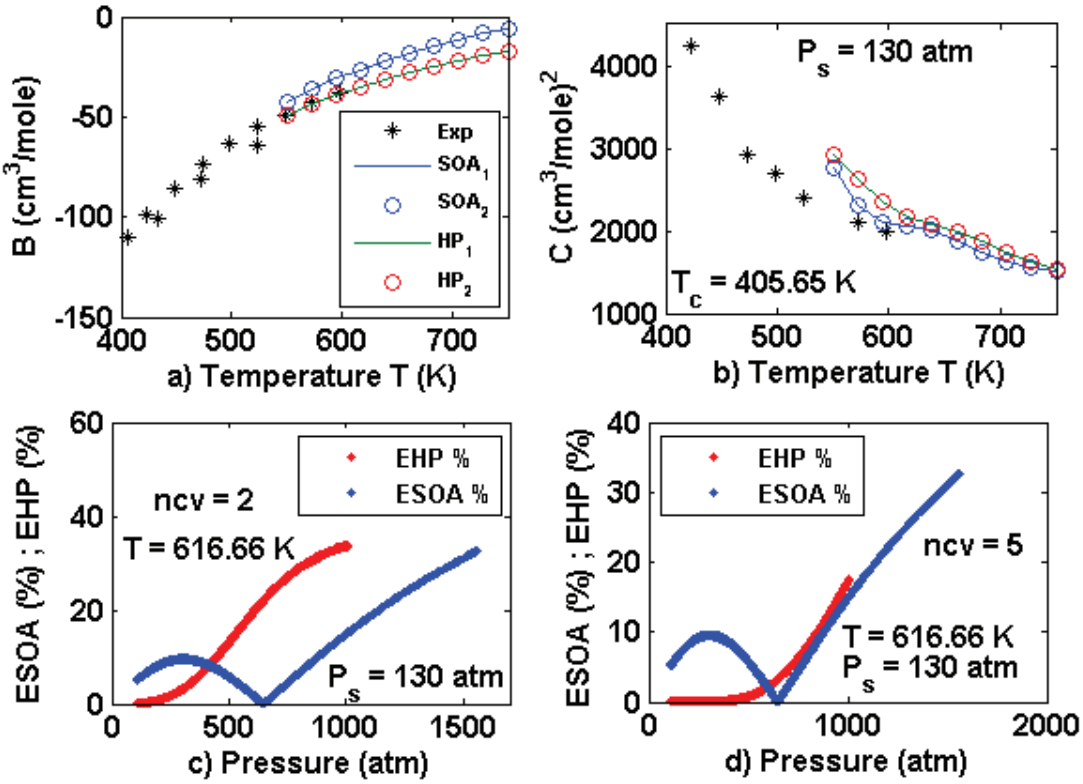
B (cm3/mole)
a) Temperature T (K)
Exp
SOA1
SOA2
HP1
HP2
C (cm3/mole)2
b) Temperature T (K)
Ps = 130 atm
Tc = 405.65 K
ESOA (%) ; EHP (%)
c) Pressure (atm)
EHP %
ESOA %
ncv = 2
T = 616.66 K
Ps = 130 atm
d) Pressure (atm)
ncv = 5

Figure 18

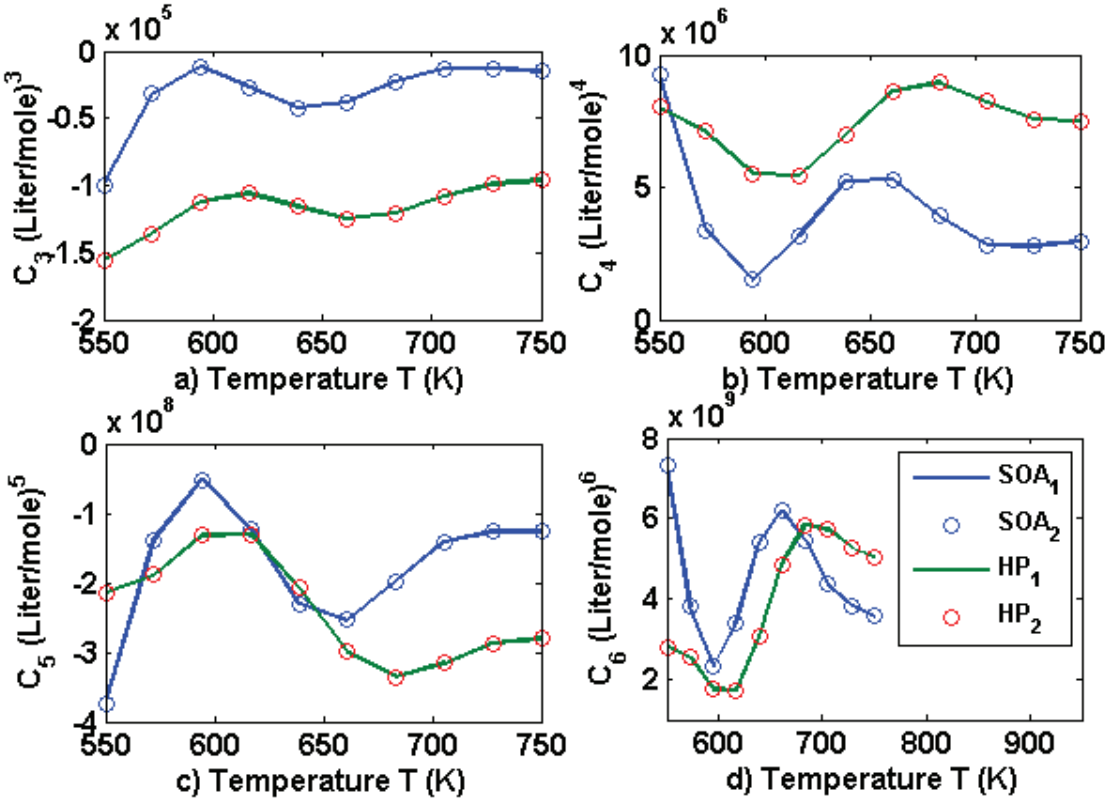
x 10^5
C3 (Liter/mole)^3
a) Temperature T (K)
x 10^6
C4 (Liter/mole)^4
b) Temperature T (K)
x 10^8
C5 (Liter/mole)^5
c) Temperature T (K)
x 10^9
C6 (Liter/mole)^6
d) Temperature T (K)
SOA1
SOA2
HP1
HP2

Figure 19

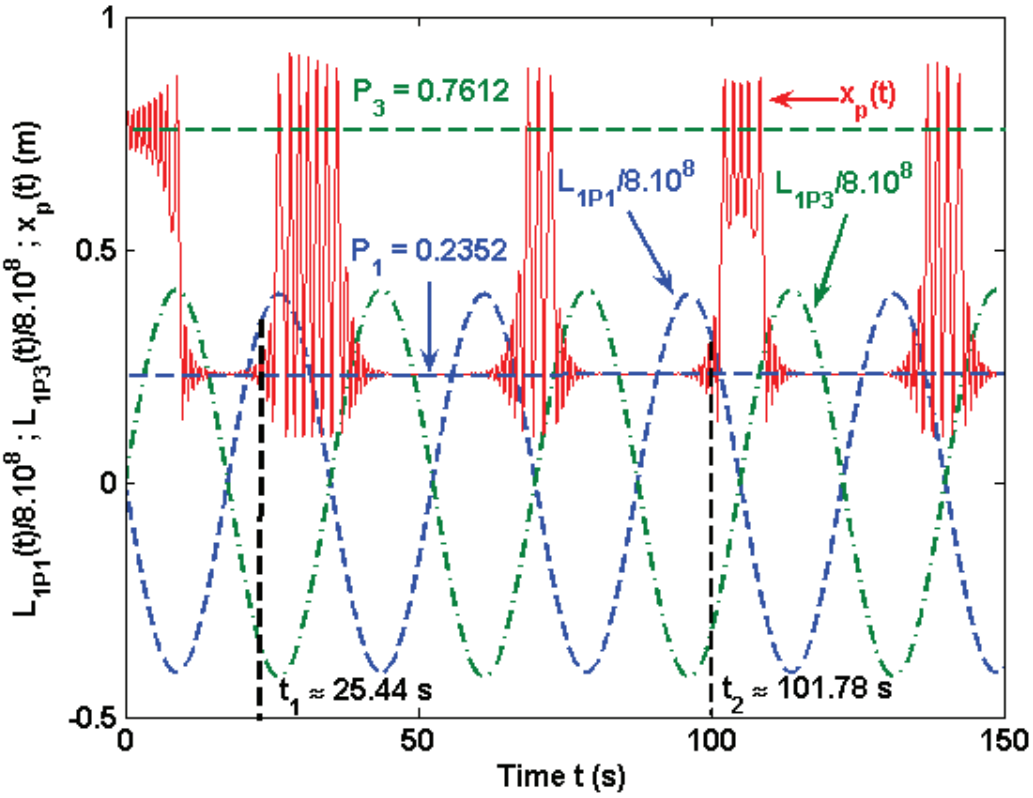
P3 = 0.7612
xp(t)
L1P1/8.10^8
L1P3/8.10^8
P1 = 0.2352
t1 ≈ 25.44 s
t2 ≈ 101.78 s
L1P1(t)/8.10^8 ; L1P3(t)/8.10^8 ; xp(t) (m)
Time t (s)
1
0.5
0
-0.5
0
50
100
150

Figure 20

Legend of Figures

Figure 1. Layout of the mobile piston inside a cylinder with nonlinear spring, damper, heating coils (C, C_1), loop 1 with a PI controller, nonlinear control loop 2 and control force F'(t). The parameter values are: L = 1m, d_c = 0.1 m, S = $7.8540.10^{-3}$ m^2, d_1 = 0.1 m, c = 0.02 m, d = 0.98 m, V_{se} = $5.6341.10^{-3}$ m^3, K_s = $7.5020.10^8$ J/m^3, α = $9.7262.10^{-11}$ m^3.mole.K/J^2, β = $1.3333.10^{-10}$ mole.m^3/J.s, K_p = $1.8268.10^{-9}$ m^3/s.K, f_c = 0.001, m = 1.1939 kg, K_1 = 311.64 N/m, K_2 = 449.84 N/m^3, K = 680.14 N/m^2, P_{1s} = 5287.7 N/m^2, b = 1 N.m/s and Q_s = 6734.6 J/s. TT, FT and PT denote the temperature, flow and pressure transmitters respectively, whereas TIC is an indicator PI controller.

Figure 2. Simulation results using the SRK state equation and the nitrogen (parameter values are indicated in the legend of Fig 1). a) Equilibrium points P_1 (stable weak focus), P_2 (unstable saddle), P_3 (stable weak focus) corresponding to Eq (23). b) Piston position as a function of the time for C_0 =-500 and C_1 = 0. c) Gas temperature as a function of the time. d) Heat flux in the helical heating coils C and C_1.

Figure 3. a) Gas pressure as a function of the time when the piston position varies as shown in Fig 2 b). b) Specific volume when the piston jumps from P_3 to P_1. c) Phase plane of the piston position when the gas temperature is almost constant as shown in Fig 2 c). d) Variation of the compressibility as a function of the pressure indicating the pressure jumps (parameter values are indicated at legend of Fig 1).

Figure 4. **S**imulation results for the SRK state equation and the methane, obtained by varying harmonically the first Lyapunov value with C_0 = 0, C_1 = -500, ω_L = 35 rad/s. a) Sensitive dependence for the gas pressures when the system is simulated with initial pressures differing in 10^{-5} atm. b) Pressure errors of Fig 4 a) as a function of the time. c) Temperatures with very small oscillations corresponding to the pressures of Fig 4 a). d) Piston position as a function of the time for the pressures, specific volume and temperatures plotted in Figs 4 a), b) and c) respectively.

Figure 5. a) Strange attractor in the phase plane of piston velocity versus piston position corresponding to the chaotic data plotted in Fig 4. b) Piston position as a function of the time when the piston motion is periodic. c) Orbit in the phase plane of the mobile piston with periodic behavior.

Figure 6. Analysis of the chaotic behaviors depicted in Figs 4 and 5 a). a) Plot of all Lyapunov exponents as a function of the time, showing that two of them are positive. b) Vector field divergence and sum of Lyapunov exponents as a function of the time. c) Power spectral density for the piston position depicted in Fig 4 d). d) Specific heats at constant pressure c_p and at constant volume c_v for the nitrogen as a function of the time.

Figure 7. Pressure simulation results for the cubic equations RK, SRK, PR and VDWt, obtained by using the same pressure P_s = *100* atm and temperatures T_s = *300* and T_s = *700 K* for the argon (parameter values are indicated at legend of Fig 1).

Figure 8. a) Specific volume as a function of the time corresponding to Fig 7 d). b) Temperature as a function of the time corresponding to Fig 7 d). c) Strange attractor in the phase plane for the piston force versus piston velocity.

Figure 9. a) Adjustment of Eq (56) for the chaotic simulation results depicted in Figs 7 a), 8 a) and 8 b) by means of a fifth-degree polynomial to estimate five virial coefficients. b) Variation of the compressibility coefficient for the argon as a function of the pressure for one (z_B) two (z_{BC}) and three (z_{BCD}) virial coefficients.

Figure 10. a) Compressibility coefficient for the argon as a function of the pressure calculated with two and four virial coefficients (z_{BC} and z_{BCDE} respectively) estimated from the data shown in Fig 9 a). b) Comparison between the compressibility coefficient z_a deduced from chaotic data and z_{BCDE} as a function of the pressure. c) Error between the different compressibility coefficients plotted in Fig 10 a). d) Error between different the compressibility coefficients plotted in Fig 10 b).

Figure 11. a) Variation of the pressure as a function of time for the oxygen, obtained through the PR state equation. b) Variation of the specific volume as a function of the time for the oxygen, obtained through the HP state equation. c) Comparison between experimental and chaotic simulation data for the second virial coefficient obtained from the PR and HP state equations. From the chaotic data, six virial coefficients are estimated. d) Comparison between experimental and chaotic simulation data for the third virial coefficient obtained from the PR and HP state equations.

Figure 12. Virial coefficients C_3 to C_6 for the oxygen estimated from the chaotic data depicted in Figs 11 a) and b) as a function of the temperature for the PR and HP state equations.

Figure 13. Relative error between the pressure for the oxygen deduced from the PR and HP state equations and the one calculated from the chaotic data with a) two virial coefficients and b) six virial coefficients. Relative error between the pressure for the methane deduced from the SRK and HP state equations and the one calculated from the chaotic data with c) two virial coefficients and d) six virial coefficients.

Figure 14. a) Relative error between the pressure for the nitrogen deduced from the RK and HP state equations and the one calculated from the chaotic data with five virial coefficients. b) Relative error between the pressure for the nitrogen deduced from the VDWt and HP state equations and the one calculated from the chaotic data with two virial coefficients. c) Variation of the gas temperatures as a function of the time obtained in the simulations of Fig 14 b). d) Heat fluxes for the HP state equation and the temperatures plotted in Fig 14 c).

Figure 15. Chaotic results for the argon obtained by applying an external harmonic disturbance and the PRt state equation: a) pressure and b) temperature. c) Strange attractor in the phase plane consisting of the piston velocity versus piston displacement.

Figure 16. Variation of the fugacity coefficient for the methane as a function of the reduced pressure, obtained at 300 K and 700 K.

Figure 17 a) Comparison between experimental and chaotic simulation data for the second virial coefficient obtained from the SOA and HP state equations for the acetone. From the chaotic data, six virial coefficients are estimated. b) Comparison between experimental and chaotic simulation data for the third virial coefficient obtained from the SOA and HP state equations for the acetone. The simulation results have been obtained by varying harmonically the first Lyapunov value with $C_0 = 0$, $C_1 = -500$ and $\omega_L = 35$ rad/s. The initial pressure is $P_s = 30$ atm and the temperature is between 550 K and 750 K.

Figure 18 Estimation of six virial coefficients from the chaotic data. a) Comparison between experimental and chaotic simulation data for the second virial coefficient obtained from the SOA and HP state equations for the ammonia. b) Comparison between experimental and chaotic simulation data for the third virial coefficient obtained from the SOA and HP state equations for the ammonia. The simulation results have been obtained by varying harmonically the first Lyapunov value with $C_0 = 0$, $C_1 = -500$ and $\omega_L = 35$ rad/s. The initial pressure is $P_s = 30$ atm and the temperature is between 550 K and 750 K. c) Relative error between the pressure obtained from the SOA and HP state equations and the one calculated from the chaotic data with two virial coefficients. d) Same as c) but with five virial coefficients.

Figure 19. Virial coefficients C_3 to C_6 for the ammonia estimated from the chaotic data depicted in Figs 17, 18 a) and 18 b) as a function of the temperature for the SOA and HP state equations.

Figure 20. Piston position and scaled first Lyapunov values L_{1P1} and L_{1P3} of the equilibrium points P_1 and P_3 as a function of the time for the refrigerant R22.